Applied Catalysis B: Environmental 217 (2017) 494–522

Contents lists available at ScienceDirect

Applied Catalysis B: Environmental

journal homepage: www.elsevier.com/locate/apcatb

Review

Recent progress for direct synthesis of dimethyl ether from syngas on the heterogeneous bifunctional hybrid catalysts

K. Saravanan [a], Hyungwon Ham [a], Noritatsu Tsubaki [b], Jong Wook Bae [a,*]

[a] School of Chemical Engineering, Sungkyunkwan University (SKKU), 2066 Seobu-ro, Jangan-gu, Suwon, Gyeonggi-do, 16419, Republic of Korea
[b] Department of Applied Chemistry, School of Engineering, University of Toyama, Gofuku 3190, Toyama, 930-8555, Japan

ARTICLE INFO

Article history:
Received 5 February 2017
Received in revised form 4 April 2017
Accepted 29 May 2017
Available online 7 June 2017

Keywords:
Syngas
Dimethyl ether
Copper-based catalyst
Alumina
Zeolites
Bifunctional (hybrid) catalysts

ABSTRACT

The recent rising demand of renewable energies and climate changes has been driving intensive academic researches into new chemical routes to sustainable and clean fuel productions in order to meet the demands of industrial evolution by solving energy crisis due to limited fossil fuel reservoirs and increasing environmental pollutants. Dimethyl ether (DME) is a multi-purpose synthetic fuel and chemical that can be used as an excellent alternative to diesel fuel and liquefied petroleum gas (LPG). The present review paper briefly provides an overview of the recent developments for a direct synthesis of DME from synthesis gas (syngas, $CO + H_2$) over some hybridized bifunctional heterogeneous catalysts composed of copper-based hydrogenation catalysts with solid acid components such as alumina or zeolites mainly, where the catalytic activities significantly depend on its properties influenced by synthesis protocols, porosities, surface areas, interactions of active metals with supports, distributions of metal particles on the supports and so on. We have also briefly covered the hydrogenation of CO_2, a model reaction for the utilization of CO_2 containing in syngas, to produce DME and thereby significantly mitigate its environmental impacts. Furthermore, the catalytic performances of the direct synthesis of DME by hydrogenation of carbon oxides were explained in terms of the acid sites of the solid acid catalysts and surface area of metallic copper nanoparticles in the hybridized bifunctional catalysts with their preparation protocols.

Contents

* Corresponding author.
E-mail address: finejw@skku.edu (J.W. Bae).

http://dx.doi.org/10.1016/j.apcatb.2017.05.085
0926-3373/

1. Introduction

The energy utilization cycle generally consists of three stages such as an energy generation, distribution and consumption, all of which must be closely balanced for an ideal energy infrastructure [1]. Meanwhile, the world energy consumption is steadily increasing, and thus rapidly depleting energy resources owing to an industrial evolution by generating significant environmental pollutants from an increasing population and globalization [2]. The conventional fossil resources such as crude oil, coal and natural (or shale) gases are the major sources of world's primary energies (Fig. 1a) that are used mostly as fuels (Fig. 1b) [3]. However, when fossil fuels are burnt they predominantly produce CO_2 that has been identified as a major source contributing to climate changes. Besides they generate other harmful gases such as SOx and NOx which need to be removed to meet the environmentally acceptable fuel requirements. To limit these unwanted harmful gas increases, some supplements of fossil fuels are prerequisite for a sustainable society [1,4]. Furthermore, the present use of natural resources does not secure the ability of future generations to meet their own energy needs. Although the exploitation of unconventional fossil fuel resources such as shale oil and shale gas could significantly increase the availability of affordable fossil fuels, the impacts of their production on the environment are also raising numerous concerns [5]. The utilization of these fossil and unconventional resources also impair the problems associated with the greenhouse gas emissions (especially, CO_2) and thus it is vital for mankind to find renewable, sustainable and environmentally friendly alternative chemicals for heat, power and transportation and so on.

A great deal of researches has been conducted to meet the rising demands for energy and to mitigate CO_2 emission by developing more sustainable technologies that use the available raw materials like coal, natural gas and biomass [4,6]. Synthesis gas (syngas, mainly $CO + H_2$ mixtures), the raw materials for clean fuels and platform chemicals, can be produced from coal, natural gas, biomass and other waste resources. Although, for economic reasons, syngas is now exclusively produced from natural gas and coal, it could be made from any carbon containing feedstock including biomass. Biomass, CO_2 neutral resource, extensively distributed in the world and it is considered as one of the alternative feedstock for the production of fuels and chemicals [7,8].

Two main chemical transformation routes were reported in the literatures for the conversion of syngas into fuels. (1) The production of linear aliphatic hydrocarbons including methane by methanation has been well known by Fischer-Tropsch synthesis (FTS) reaction which can be catalyzed by the supported transition metals such as Ru, Fe and Co. (2) Syngas to methanol which gives dimethyl ether (DME) by dehydration. Both the above routes have been successfully implemented in industry for the production of synthetic fuels [9]. However the former method should require CO_2-free syngas, whereas methanol/DME synthesis route can be conducted in the presence of CO_2-rich syngas and thus it has been considered as a promising method to get synthetic clean fuels and to mitigate CO_2 emission. Both methanol and DME can be used as synthetic fuels. Nevertheless, DME provides a high H/C ratio with relatively harmless. Therefore, DME is more preferable and often plays an alternative role to methanol [10]. DME, also called as methoxymethane (CH_3OCH_3), the smallest aliphatic ether, is a non-toxic, non-carcinogenic and non-corrosive compound. DME can be used as an excellent alternative to diesel fuel due to its high cetane number (55–60) and a low emission of CO, NOx in the exhaust gases from a diesel engine as it has no C—C bond structures. It also has similar physical properties as that of liquefied petroleum gas (LPG) and hence can be used as an alternative fuel for cooking and heating [11a]. Furthermore, the well-developed infrastructures of LPG can be adapted for DME and this makes DME outstanding for practical uses [10]. As multisource, multi-purpose clean fuels, it is also projected as a chemical feedstock of the 21st century for the production of hydrocarbon, oxygenates and higher ethers [7]. For instance, there is a huge market value for acetic acid, gasoline and olefins which can be possibly derived from DME (Fig. 2). Since DME having a high H/C ratio and intense energy density, it can be used

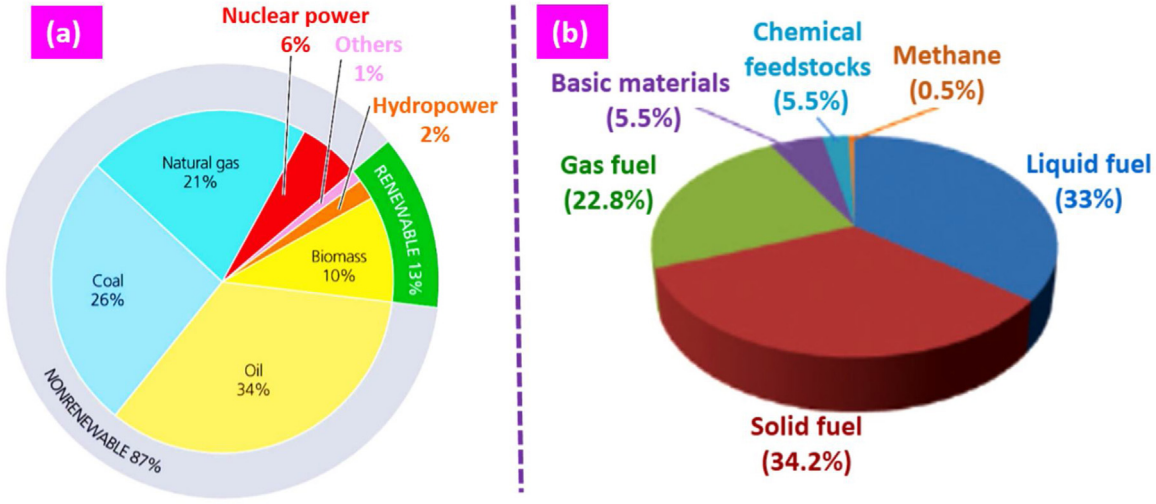

Fig. 1. (a) World's primary energy resources and (b) their uses [modified form of Ref. [3]].

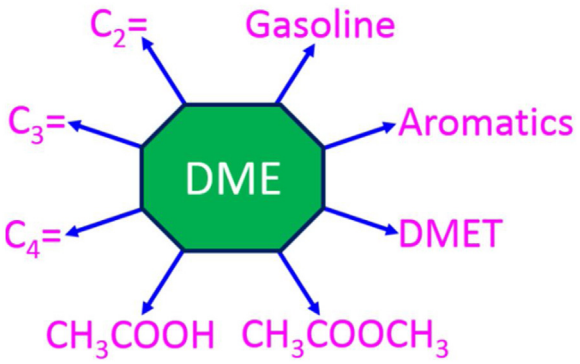

Fig. 2. DME as an intermediate for various hydrocarbon and oxygenate products.

for hydrogen and dimethoxyethane (DMET) production by steam reforming (or partial oxidation) and steam plasma, respectively [11]. DME is an excellent solvent and also degrades rubber materials [12]. It has also been increasingly used as an aerosol propellant to replace conventional chlorofluorocarbons which are found to destroy ozone layers of the atmosphere [13]. The DME aerosol propellant has been used in a wide range of personal care products including shaving creams, hairspray, foams, and antiperspirants because of its higher water solubility relative to other propellants. Besides, DME has been used in a limited amount to freeze meat and fish by direct immersion [12].

DME was firstly appeared in 1867 as an anesthetic agent that tested in rabbits and pigeons [12]. In 1963, Akzo Nobel Corporation firstly used DME as an aerosol propellant. In 1970s, oil prices were increased, and significant efforts have been made to produce cleaner diesel fuels and other alternative fuels [14]. From the late 1970s, a global oil company called Amoco has started work on the production of liquid fuels from syngas. Majunke and Mueller filed a German patent in 1984 where they pointed out "methanol based fuel consisting of DME" [15]. Following this patent, a US patent published on "method of operating a diesel engine with a fuel consisting of >95% DME" in 1990 [16]. In the late 1990s, Amoco jointly collaborated with the General Electric Co. (GE) and the Electric Power Development Corporation (EPDC) of Japan tried DME as a "gas turbine fuel". DME production was efficiently performed in this test and it showed low emissions of particulate matter as well [12]. As shown in Fig. 3, the history of DME production and its established milestones was summarized into early and developing stages from 1963 to 1990 and active stage after 1990s. In the subsequent years, several publications on DME synthesis were reported using single-step method over homogeneous and heterogeneous catalysis (Fig. 4). Similarly, a lot of citations on DME synthesis are exponentially increasing every year as summarized in Fig. 4.

This topic was first reviewed in 2006 by Semelsberger et al. [18] on the viability of DME as an alternative fuel. Two reviews (2008 and 2014) were described the potential usage of DME in compression-ignition engines [19]. Yoon and Han pronounced some technological and economic aspects of DME production and its future uses [20]. In 2010, two short-reviews were published on catalyst development for the production of DME [7,21]. Fleisch et al.[22] described the history and status of DME as an alternative fuel. Recently, Bhattacharya et al. [23] reviewed on the current and potential future applications of Victorian brown coal for DME synthesis. Very recently, two reviews were summarized in 2014 on the catalysts and reactors used for the production of DME [24,25]. Among them, the last two review papers were covered the technologies in reactor design and randomly chosen hybrid/bifunctional catalysts for syngas to DME synthesis [24,25] that are inadequate in a catalysis point of view, while others just mention DME as potential alternative fuel [18,19a,22], but this area has been progressing very fast, and over 200 articles have been published in scientific journals from 2006 to 2016 (Fig. 4). In this review paper, we try to provide an overview of the recent developments in the direct synthesis of DME from syngas (CO (or CO_2) + H_2) over typical heterogeneous hybrid/bifunctional catalysts, where syngas to DME performance was well correlated with the acid sites of the solid-acid catalysts as well as the metal particle surface areas in the hybridized bifunctional catalysts.

2. Methods for synthesis of DME

DME synthesis can be categorized into a single-step process and two-step process. The former and the latter are named as the direct synthesis and the indirect synthesis, respectively [26]. In the conventional indirect synthesis, methanol is synthesized from syngas (Eq. (1)) on a metallic copper-based heterogeneous catalyst (mainly, $Cu/ZnO/Al_2O_3$) in the first step through CO hydrogenation, which is limited thermodynamically, especially at high reaction temperatures [27]. In the second step, methanol is dehydrated into DME (Eq. (2)) over solid acid catalysts (Fig. 5) such as γ-alumina, zeolite and mixed metal oxides and so on.

$$CO + 2H_2 \leftrightarrow CH_3OH \quad \Delta H^o = -90.6\,kJ/mol(CO\ hydrogenation) \quad (1)$$

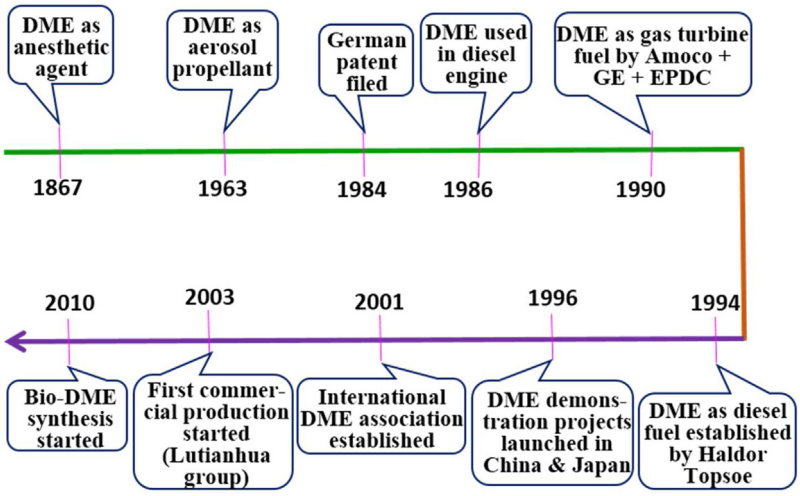

Fig. 3. History, development and milestones of DME production.

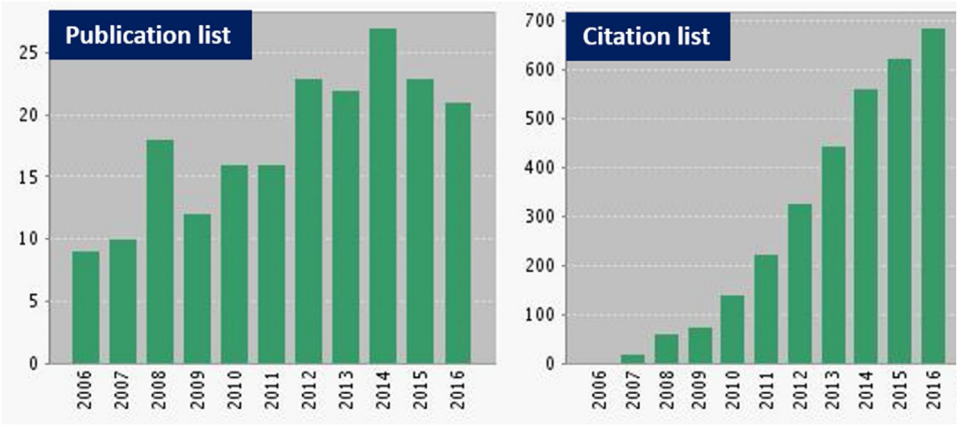

Fig. 4. Number of articles published and cited on DME synthesis in the presence of catalysts [17].

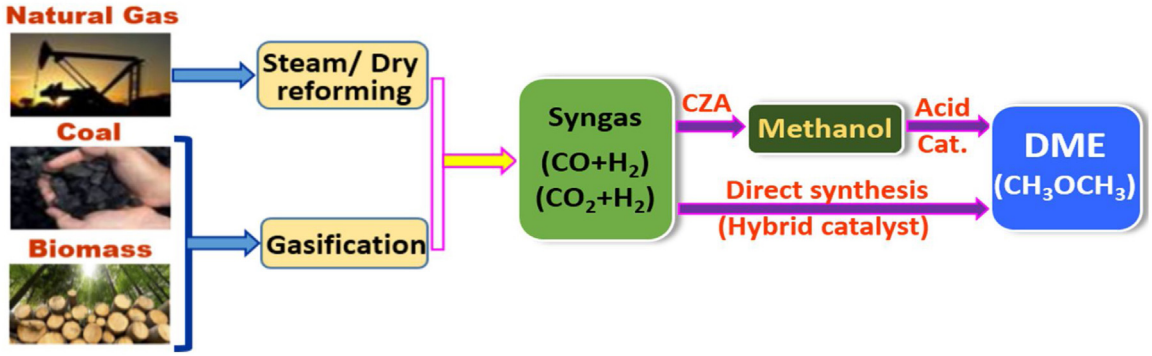

Fig. 5. Simplified schematic representations of indirect and direct synthesis process for DME production from syngas.

$$2CH_3OH \leftrightarrow CH_3OCH_3 + H_2O \quad \Delta H^o = -23.4\,kJ/mol$$
(dehydration of CH_3OH) (2)

On the other hand, the direct DME synthesis from syngas, one of the products in each step is a reactant for the other, is an attractive alternative to the two-step process [28]. For example, hydrogen formed as in Eq. (3) is a reactant for the methanol synthesis. The direct DME synthesis, which simultaneously triggers methanol synthesis and *in-situ* dehydration, is integrated in hybrid catalysts in a single reactor (Fig. 5), alleviates the thermodynamic constraints of methanol synthesis leading to higher CO conversion and higher DME selectivity [26,27,29]. In general, a higher one-pass syngas conversion and lower hydrogen demand (possibly at below H_2/CO ratio) in the feed stream with lower thermodynamic limitations and higher economical and theoretical significances make the single-step synthesis of DME from syngas attractive industrially. Also the usages of a single reactor without purification and transportation units of methanol should reduce the capital costs for the DME production [30]. In the direct synthesis, however, not only methanol synthesis and dehydration but also water gas shift (WGS) reaction can be simultaneously involved (Eq. (3)) [29]. Accordingly, the total net reaction in the direct synthesis of DME is given in Eq. (4).

$$H_2O + CO \leftrightarrow H_2 + CO_2 \quad \Delta H^o = -41.2\,kJ/mol(WGS) \tag{3}$$

$$3CO + 3H_2 \leftrightarrow CH_3OCH_3 + CO_2 \quad \Delta H^o = -245.8\,kJ/mol$$
(total net reaction) (4)

On the other hand, the following methanol synthesis reaction by CO_2 hydrogenation is involved when CO_2 is contained in syngas [31].

$$CO_2 + 3H_2 \leftrightarrow CH_3OH + H_2O \quad \Delta H^o = -49.5\,kJ/mol(CO_2 hydrogenation) \tag{5}$$

Eq. (5) clearly indicates that CO_2 utilization can be achieved in methanol synthesis. Based on the thermodynamic calculation, since a less heat is liberated from Eq. (5) as compared to Eq. (1), adding CO_2 into syngas is able to suppress the increase in temperature and avoid overheating phenomenon in the catalyst-bed and thus enhancing its thermal stability [28b]. Although the aforementioned merits of the direct usages of CO_2-containing syngas, H_2O is also generated, as expressed in Eq. (5), that may reduce the catalytic stability and DME yield [32].

In order to understand the equilibrium limits imposed in conversion of syngas to DME and other byproducts, a thermodynamic analysis was made by us using HSC Chemistry software. Equilibrium conversions and product compositions for both CO and CO_2 hydrogenation reactions at the molar ratio of H_2:CO = 2:1 and H_2:CO_2 = 3:1 and pressure of 50 bar at different temperatures are shown in Fig. 6. Since the conversion of syngas to DME is highly exothermic (Eq. (4)), the formation of DME is thermodynamically favored at low temperature for both CO and CO_2 hydrogenation reactions (Fig. 6). Thermodynamic analysis of CO hydrogenation reaction clearly shows that the DME is the most favored product. It can deduced from the CO_2 hydrogenation reaction that increasing the reaction temperature (>280 °C) does not favor the formation of any byproducts. It is also important to mention that the real direct DME synthesis product distribution may not correspond to the predicted values by thermodynamics. The product distributions are controlled by kinetics, however, a good understanding of the

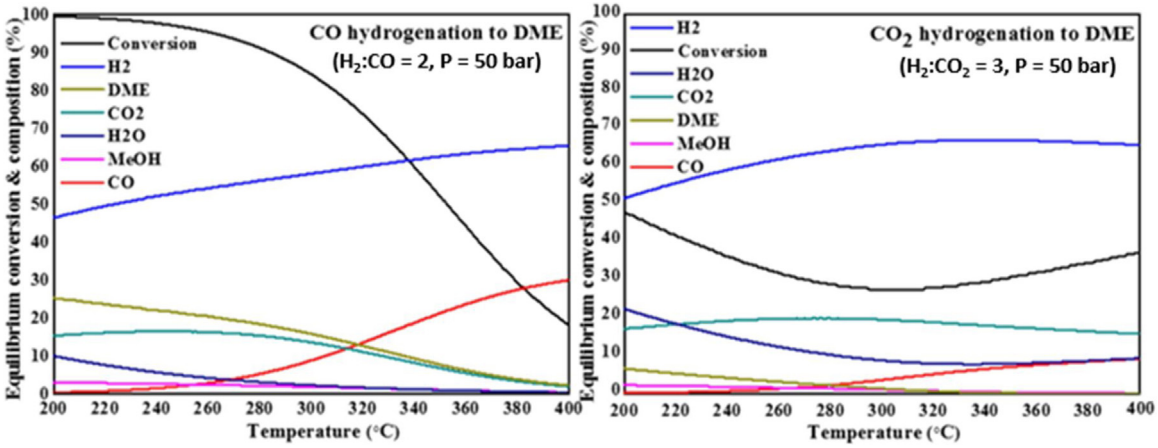

Fig. 6. Equilibrium conversions and product compositions with varying reaction temperatures for carbon oxides hydrogenation reaction (thermodynamic analysis by HSC Chemistry software).

thermodynamic limitations for direct DME synthesis reaction from syngas can be useful for developing new chemical processes and improving old ones.

2.1. Important parameters in DME synthesis

The reaction parameters, such as temperature, pressure, space velocity, and H_2 to COx ratio, and CO_2 content in the feed stream as well as type of reactors are known to affect both conversion of COx and DME selectivity. The details of these parameters were already discussed well in the previous review paper published by Azizi et al. [25]. It is also an important parameter that the well-designed catalysts are needed to enhance DME selectivity. The direct DME synthesis requires the combination of two catalytic functions (*i.e.* hybrid/bifunctional catalyst): a metallic function that catalyses the hydrogenation of COx, and an acidic function to catalyse the dehydration of methanol to DME. In the following sections relevant those catalysts of methanol synthesis and dehydration to DME are briefly reviewed.

2.1.1. Cu-based catalyst for methanol synthesis

The first commercial catalyst for converting syngas to methanol was demonstrated by BASF in 1923 using ZnO—Cr_2O_3 catalyst which are only active at high temperature (350–400 °C) and high pressure (240–350 bar) to reach acceptable conversion [33]. However this catalyst easily poised with syngas containing impurities like sulphur, chlorine and heavy metals. Imperial Chemical Industry (ICI) introduced the more active and stable Cu/ZnO based catalyst in 1966 [28a]. ZnO promoter acts as a geometrical spacer between Cu nanoparticles and thus plays a pivotal role in maintaining the active Cu metal in optimal dispersion in the Cu/ZnO catalyst, consequently providing a high number of active sites exposed to gaseous reactants [32]. Behrens et al. [34] have reported that ZnO can promote strong metal–support interaction with Cu species, which induces the formation of 'methanol-active copper'. Furthermore, addition of trivalent ions like Al^{3+} into the Cu/ZnO was found to improved stability along with Cu dispersion and metal surface area. Afterwards, a ternary Cu/ZnO/Al_2O_3 (CZA) catalyst started to use for methanol synthesis operating at moderate pressure ranging from 50 to 100 bar and temperature ~250 °C [23,28a]. Since then, Cu/ZnO catalytic system promoted by several other irreducible oxides for methanol synthesis has undergone few modifications (Fig. 7) although some extensive researches haven been taking place to find new catalytic routes to work at even lower temperatures and pressures [35].

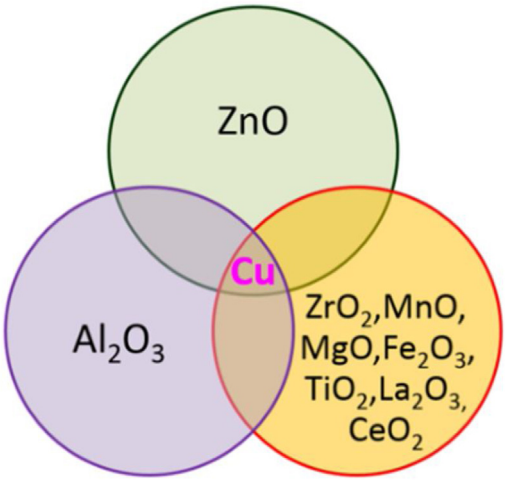

Fig. 7. General combinations of the supports used for Cu-based heterogeneous catalysts for the hydrogenation of carbon oxides (CO and/or CO_2) for methanol synthesis.

2.1.2. Solid acid catalyst for methanol dehydration

An ideal solid acid catalyst should have high stability, necessary acid sites, hydrophobic surface, low cost, high activity and selectivity for desired products. Solid acid catalysts namely alumina and zeolites have been mainly used for methanol dehydration to form DME selectively. Methanol dehydration reaction is believed to be catalyzed by the weak to moderate acid sites such as Lewis and Brønsted acid sites [36]. Alumina forms Lewis acid-base pair during calcination. Sung et al. [37] carried out the methanol dehydration reaction with different crystalline phases of alumina and found that γ-Al_2O_3 showed the highest activity for methanol to DME conversion than that of α- and κ-Al_2O_3. The structure of γ-Al_2O_3 is traditionally considered as a cubic defect spinel type ($MgAlO_4$) at which Mg^{2+} ions are replaced by Al^{3+} ions (67%) and vacancies (33%) to give an overall formula of Al_2O_3 [9]. However, the surfaces of γ-Al_2O_3 remain with an excess of positive charge that is compensated by hydroxyl anions (OH^-). Such hydroxyl anions are weakly acidic but dehydration at high temperatures create coordinatively unsaturated metal cations and oxide anions that can act as Lewis acid and basic sites, respectively as shown in Fig. 8 [38].

Although γ-Al_2O_3 exhibits a remarkable selectivity towards DME, many hydrophobic zeolites show much better performance in terms of catalytic activity and stability, especially in presence of water [39]. Zeolites, which are the microporous crystalline solid

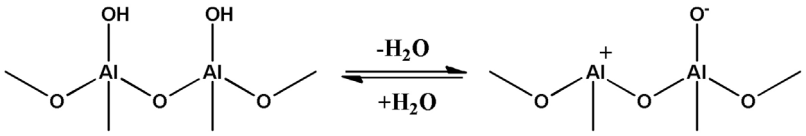

Fig. 8. Surface dehydration/hydration reactions in the γ-Al_2O_3 [9,38].

Table 1
Structures of commonly used methanol dehydration zeolite-based catalysts and their micropore networks with pore arrangements [9,43].

Zeolite type	Structures	Micropore networks	Pore arrangement
Mordenite	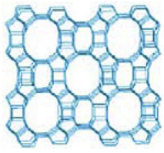	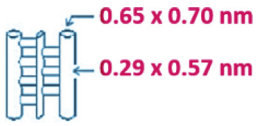	2-dimensional pore system (straight 12-memdered ring channels connected by short alternating 8 membered ring channels)
ZSM-5	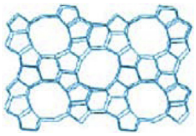		3-dimensioanl pore system (straight 10-membered ring channels connected by sinusoidal channels)
Ferrierite		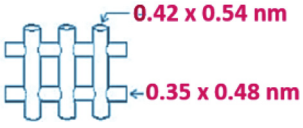	Orthorhombic pore structures (10-membered ring channels perpendicularly intersected with 8-membered ring channels)

acids with well-defined pore structures containing Al, Si and O species in their frameworks, exhibit Brønsted-type acid-base properties mainly [40]. The distribution of the acid strengths among the proton donor groups in the zeolites could vary largely. For instance, the acid sites of mordenite and ZSM-5 are significantly stronger than faujasite [41]. Generally, the structure of zeolites can be classified as 1-, 2- and 3-dimensional and may comprise complicated channels (interconnected or separated) or cages. The micropores of zeolites are typically constructed from 12-, 10- and 8-member-rings, and sizes of the pores are categorized as an approximately 0.7 nm (large, mordenite), 0.55 nm (medium, ZMS-5) and 0.4 nm (medium to small, ferrierite), respectively [42]. The structures with their micropore networks along with pore arrangements of zeolites can typically change methanol dehydration activity as summarized in Table 1.

It is worthy to be noted that during the dehydration of methanol to DME formation, hydrocarbons may also be formed as byproducts in a consecutive reaction which involves a combination of DME condensation, methylation and olefin elimination (Eq. (6)). The chain length of the hydrocarbons formed increases with the acidity of the catalysts (*i.e.* acid sites and strength) and the reaction conditions such as temperature, pressure and space velocity of syngas-to-DME (STD) [9]. For instance, the selectivity towards light olefins (C_nH_{2n}) found by using low acidic catalysts, and paraffins and aromatic compounds formed via hydride transfer and cyclization reactions, respectively, over strongly acidic catalysts at operating temperatures above 300 °C besides coke formation. Therefore, optimum acid strength and density of the acid sites along with the reaction conditions are very important factors to reduce the hydrocarbon formation either by formed DME or methanol.

$$(n/2)[2CH_3OH \leftrightarrow CH_3OCH_3 + H_2O] \rightarrow C_nH_{2n} + nH_2O \rightarrow \text{aromatics or paraffin} \quad (6)$$

2.1.3. Hybrid/bifunctional catalysts

The conversion of syngas to DME is conducted over dual catalytic systems comprising of a physical mixture of methanol synthesis catalyst (denoted as MSC) and methanol dehydration catalyst (denoted as MDC), generally called bifunctional or hybrid catalyst, or over a hybrid catalyst prepared via coprecipitation or mixing of the freshly precipitated precursors in which the two catalytic functionalities are constructed into a single entity (*i.e.* shorter contact distance). As in any hybrid catalytic systems, the two catalytic functions can work in a complete "synergistic effect" through being finely dispersed by maintaining a close proximity but not reacting each other in order to maximize DME productivity during the STD process [9,29,44–46]. However, the catalytic performances of the hybrid catalysts mainly depend on the dispersion of Cu nanoparticles of the MSC and the nature of acidic properties of the MDC. Hybrid catalyst has also been synthesized by coprecipitation, impregnation, coprecipitation-sedimentation, sol–gel, sol–gel impregnation and liquid–phase synthesis. The information on these preparation methods have been so voluminous that are already reported by Bhattacharya et al. [23] and it is beyond scope of the present review. Very recently, some advanced methods like colloidal approach [47], combined coprecipitation ultrasound [48] and flame spray pyrolysis [49] were also reported for STD synthesis in the literatures.

3. Syngas-To-DME (STD) synthesis over hybrid/bifunctional catalysts

Carbon oxides are relatively inert molecules and their chemical transformations to other ones are energetically unfavorable. However, those reactions that yield stable molecules like DME can be viable under suitable reaction conditions. Hydrogenation of CO and/or CO_2 is one of the best examples of such feasible conversions. Furthermore, when the methanol/DME production processes are considered, CO reactant is much more favorable to be converted and thus industrial hydrogenations normally use CO rather than CO_2 reactant [9].

Table 2
$Cu/ZnO/Al_2O_3$ with γ-Al_2O_3 catalyst for STD reaction.

Preparation method[a]		Reaction conditions and catalytic activity							Ref.	Notes
MSC	Bifunctional catalyst	H_2:CO ratio	T (°C)	P (bar)	Space velocity	X_{CO} (%)	Y_{DME} (%)	S_{DME} (%)		
Cml	PM	2:1	240	50	1100 mLn/gcat/h	53.3	34.3	58.3	[50]	Influence of dehydration catalyst studied
Cml	PM	2:1	250	51	–	68.0	–	66.8	[51]	
Cml	PM	2:1	260	50	4000/h	43.5	52.6	–	[52]	Effect of H_2O studied
Cml	PM	1:1	260	50	10000/h	~47	–	~65	[53]	Effect of alumina particle size studied
Cml	–	–	260	60	–	86.0	–	–	[54]	Modelling of a slurry reactor studied
Cml	PM	2:1	290	50	7500 Nml/gcat/min	~95	~52	–	[55]	Integrated micro packed bed reactor-heat exchangers studied
–	PM	2:1	260	50	1000/h	69.2	60.0	–	[56]	Simulation of fixed bed reactor studied
CP	WM	3:1	275	30	–	65.1	61.2	–	[57]	Co-feeding water to attenuate deactivation studied
CP	WM	3:1	275	30	–	–	39.0	–	[58]	Deactivation study conducted
CP	PM	1:1	250	30	100 mL/ min	~40	–	~10	[59]	Effect of water on liquid phase DME studied
CP	Slurry	~1:1	250	40	11000 1/h	34.1	–	49.7	[29]	γ-Al_2O_3 prepared by sol-gel and precipitation methods
CP	Slurry	2:1	250	50	2000 L/kgcat/h	49.5	–	50.3	[60]	γ-Al_2O_3 prepared from aluminum-carbon black
CP	AM	2:1	260	20	2400 mL/ g/h	~13	46.4	–	[61]	Many acid catalysts screened
CP	AM	–	250	42	6000 mL/gcat/h	~78	42.5	~66	[62]	η-Al_2O_3 also studied

[a] The bifunctional catalysts were prepared by using various solid acid catalysts through different methods as follows; Cml – commercial; CP – coprecipitation; PM – physical mixing (MSC and MDC prepared separately and then mixed together physically); WM – wet mixing; AM – admixed (MSC and MDC prepared separately and then kneading both the components to form a homogenous mixture).

3.1. Hydrogenation of CO by Cu-based MSC and γ-Al_2O_3-based MDC

3.1.1. $Cu/ZnO/Al_2O_3$ with γ-Al_2O_3 catalyst

With regard to STD process, many research groups have adopted the simple physical mixing of the CZA catalyst, commercial (Cml) or laboratory made, and γ-Al_2O_3 (Table 2). In general, conversion of CO (~53 to 95%) and DME yield (~34 to 52) was increased by increasing the reaction temperature (240 – 290 °C), although H_2:CO ratio (2:1) and pressure (50 bar) was kept constant, over commercial CZA mixed with γ-Al_2O_3 catalyst [50–62]. Although the commercial CZA catalysts showed an appreciable CO conversion, they deactivate rapidly in a slurry-phase reactor owing to detrimental interaction between the MSC and MDC [63]. This detrimental interactions may also occur during the catalyst preparation or calcination stages [64]. A series of experiments were conducted by Kim et al. [65] for STD over commercial and lab-made Cu-Zn-based catalysts and found that the hybrid catalyst, which was prepared via the coprecipitation method with a similar molar ratio of Cu/Zn to those of the commercial catalysts, showed a high activity in the direct synthesis of DME from syngas.

Though the preparation method of the catalyst for STD has a significant effect on the performance of the process [30b,44,45,64–67], the large number of variables involved in the different preparations and the lack of systematic studies has originated controversy about which method produces the most efficient hybrid catalyst. In general, routes for the coprecipitation or freshly precipitated precursors permits a close proximity, but not react, between the two catalytic functions by enhancing the "synergetic effect" and by leading to higher CO hydrogenation rates than the catalysts obtained from physical mixing method. However, this is not always the case and, in fact, several examples can be found in previous studies reporting the opposite behavior [66]. For example, Naik et al. [64] found that the catalyst prepared by a physical mixing of the two catalytic components showed a higher conversion of CO than the coprecipitation method. In parallel, Moradi et al. [45] prepared a number of CZA based hybrid catalysts by following different methods namely coprecipitation impregnation, coprecipitation-sedimentation, sol-gel and sol-gel impregnation. They observed that sol-gel impregnation method showed a higher performance in terms of CO conversion and DME selectivity. In contrast, few researchers found that the coprecipitation or coprecipitation sedimentation is best method for preparation of CZA based catalysts [30b,68–71].

Besides, the Cu-based MSC preparation methods, our research group prepared two different types of γ-Al_2O_3 [29]; one prepared by a precipitation method and the other prepared by a sol–gel method. We have obtained the best yield of DME with concomitant decrease in the CO_2 formation over the hybrid catalyst containing γ-Al_2O_3 prepared by the sol–gel method. Recently, our group also prepared a mesoporous γ-Al_2O_3 having a pore size of ~25 nm from the composite of aluminum precursor with carbon black [60]. The crucial issue for preparing a highly active hybrid catalyst is optimizing the compositions and reaction conditions of two functional components. It was observed by Abu-Dahrieh et al. [61] that the most suitable ratio between the metal and acid function was 1:1 for CZA/γ-Al_2O_3 and 3:1 for CZA/HZSM-5 admixed catalysts under the conditions studied. Jia et al. [53] claimed that the addition of dehydration catalyst to CZA resulted in a significant synergistic effect on the overall syngas conversion. For instance, the conversion of CO was found to be ~22% without γ-Al_2O_3, which significantly enhanced to ~47% with addition of 0.2 g γ-Al_2O_3 on

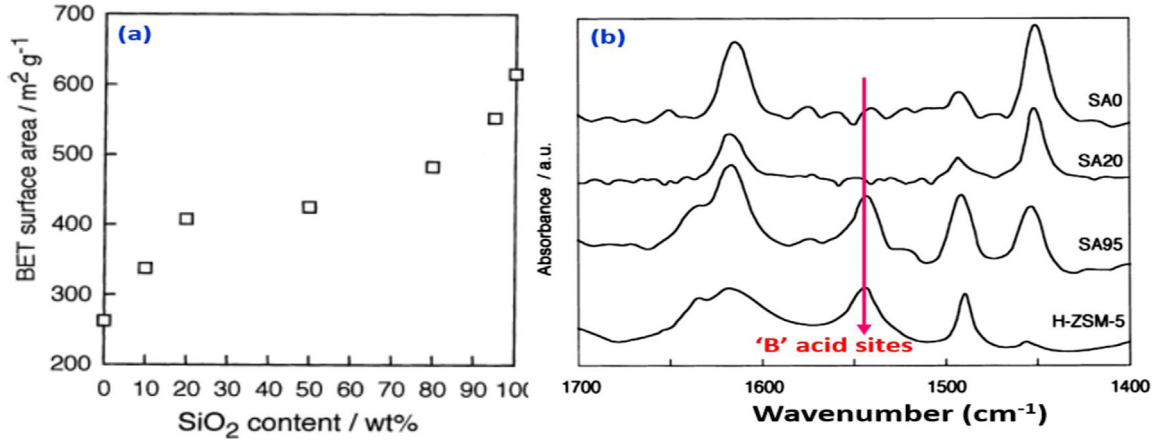

Fig. 9. (a) BET surface area and (b) pyridine FT-IR spectra of the silica-alumina (SA) samples with various silica contents [75].

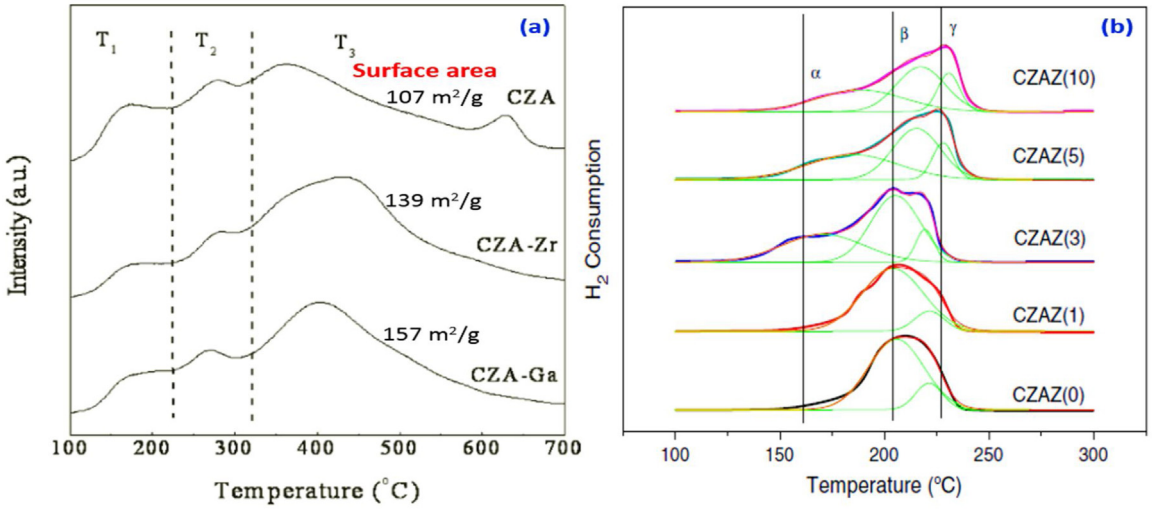

Fig. 10. (a) NH_3-TPD and surface area of the calcined Zr and Ga promoted and unpromoted CZA/γ-Al_2O_3 bifunctional catalyst [84] and (b) H_2-TPR profiles of CZAZ(x) catalysts with different Zr loadings [86].

CZA. However CO conversion decreased rapidly (~30%) by increasing γ-Al_2O_3 loadings from 0.2 g to 1 g. Unlike the conversion of CO, DME selectivity increased with increasing γ-Al_2O_3 amounts until 1 g and remained steady afterwards till 3 g.

3.1.2. *Cu/ZnO/Al_2O_3 with modified γ-Al_2O_3 catalyst*

Because the CZA-based MSC is industrially applied and is, therefore, highly matured, most of the research efforts that are being devoted to the development of active, selective, and stable STD catalysts are focused on the optimization of the MDC [72]. The research conducted so far claimed that DME formation is governed by weak to medium acid sites and those catalysts with strong acid sites may further convert formed DME to light olefins that finally causes for coke depositions [50,73]. Although the γ-Al_2O_3 exhibits an appreciable selectivity to DME during STD process, methanol and water can compete with each other for the same sites on γ-Al_2O_3, which induce a lower activity than zeolites. The catalytic activity of alumina reduces due to the fact that it has a stronger affinity to interact with water than methanol [74]. Hence, considerable attention has been recently paid toward the research on the modification of the existing dehydration component or finding new one for STD process. In order to enhance the catalytic activity and stability of alumina, different kind of modifications have been made by many researchers. As shown in Table 3, metal oxides such as silica [75], niobia [76], and anions namely fluorine [77], sulfate [78] and phosphate [79] modified γ-Al_2O_3 seem to show improved catalytic activity, compared to the pure γ-Al_2O_3.

Takeguchi et al. [75] have studied the STD reaction over the physically mixed Cu/ZnO/Al_2O_3/Cr_2O_3/Ga_2O_3 and silica-modified γ-Al_2O_3 (SA) catalysts. They concluded that silica loading results in an increase of surface area and Brønsted (B) acid sites (Fig. 9) and the modified alumina exhibits better catalytic performance. Modification with niobia on γ-Al_2O_3 decreased both the amount of basic hydroxyl groups in γ-Al_2O_3 and the irreversibility of the interaction of the catalyst surface with CO [76]. It was confirmed that both surface area and acidity of alumina are enhanced by the treatment with 0.1 mol/l NH_4F solution [77]. Mao et al. [78] studied a series of γ-Al_2O_3 samples modified with various amounts of sulfate (0–15 wt.%) and calcined at different temperatures range of 350–750 °C. They found that the hybrid catalyst containing 10 wt% sulfate and calcined at 550 °C having larger number of acid sites of moderate strength exhibited the highest DME yield of 58.3% (Table 3). Joo et al. [80] proposed that the small amount of the strong acid sites on γ-Al_2O_3 promote reforming reactions of methanol and dimethyl ether to carbon oxides. To remove the strong acid sites, the effect of the treatment of γ-Al_2O_3 and HZSM-5 with formaldehyde and sodium carbonate were studied and the modified hybrid cat-

Table 3
Commercial Cu/ZnO/Al_2O_3 with modified γ-Al_2O_3 catalyst for STD reaction.

MDC	Reaction conditions and catalytic activity							Ref.	Notes
	H_2:CO ratio	T (°C)	P (bar)	SV	X_{CO} (%)	Y_{DME} (%)	S_{DME} (%)		
Silica/γ-Al_2O_3	2.2:1	270	50	4200/h	–	55.5	93.6	[75]	Silica rich alumina showed higher activity
Nb/γ-Al_2O_3	2:1	265	50	–	8.0	–	64.9	[76]	5.9% Nb on alumina was best
F/γ-Al_2O_3	2:1	250	40	1500 mL/h/g	93.6	65.9	–	[77]	0.1 mol/l NH_4F solution performed best in STD
SO_4^{2-}/γ-Al_2O_3	2.2:1	260	40	1500 mL/g/h	94.7	58.3	61.6	[78]	10 wt.% SO_4^{2-} loaded alumina was optimized
Na_2CO_3 + HCHO treated γ-Al_2O_3	1.2:1	260	54.4	4500 mL/h/ gcat	61.1	48.4	78.6	[80]	Modified catalysts minimized the reforming reaction to CO_2

alysts minimized reforming reaction and enhanced the selectivity to DME owing to the increased amounts of weak acid sites.

3.1.3. *Modified Cu/ZnO/Al_2O_3 with γ-Al_2O_3 catalyst*

In CZA, alumina played a significant role as a promoter during methanol synthesis. Alumina inhibits thermal sintering of the Cu particles, prevents poisoning of the active metal surface and ensures additional chemical and thermal stability, which is very important for the industrial catalysts. Moreover, addition of structural promoter of Al_2O_3 on the Cu-based catalyst leads to higher intrinsic activities [81–83]. The research has also focused on the Cu metallic functions in the hybrid catalyst by adding other promoters such as Zr [84–86], Ga [84,85], Mn [87,88], Pd [28b], La [44,85], Y [85], magnesia [27], gallia with chromia [75], and carbon nanotubes [89] modified CZA (Table 4) are also able to beneficially affect the Cu dispersion, stability, activity and selectivity to DME.

For example, Venugopal et al. [85] compared the catalytic activity of the admixed catalysts composed of CZA modified with Ga, La, Y, Zr metals and γ-Al_2O_3. Results showed that yttrium (Y) modified CZA catalyst gave the highest CO conversion (~70%) and DME yield of 47.7% attributed to the addition of Y prevented the Cu particle grain growth and increased the Cu surface area. Our group examined the activity of the Zr and Ga promoted CZA/γ-Al_2O_3 bifunctional catalyst for DME synthesis from syngas [84]. In the case of the unpromoted CZA catalyst, the Cu surface area and acidity assigned to the peaks of T_1 and T_2 in NH_3-temperature programmed desorption (NH_3-TPD) are lower than those of promoted bifunctional catalysts (Fig. 10a) and resulting in showing a low DME yield (~27.0%) and CO conversion of 61.1%. The higher CO conversion (72.3%) and DME yield of 40.3% (Table 4) were observed on the CZA-Zr catalyst. Furthermore, the Zr promoter largely increased the dispersion of CZA particles on γ-Al_2O_3 by forming a strong ZrO_2—CuO interaction originating from oxygen vacancies of ZrO_2. The Ga promoter also enhanced catalytic property by the inverse spillover of hydrogen, with a less promoting effect compared to the Zr promoter [90]. Song et al. [86] suggested that an excess addition of ZrO_2 (≥5 mol%) reduced the Cu surface area and Cu dispersion and finally increased the Cu crystallite sizes. H_2-temperature programmed reduction (H_2-TPR) profile of ≥5 mol% ZrO_2 samples, CZAZ(5) & CZAZ(10), exhibited higher amounts of bulk CuO species (γ) in comparison with other ZrO_2 added samples having highly dispersed CuO species (α and β) (Fig. 10b).

The Mn-modified CZA catalyst found to have higher conversion and DME selectivity and increases better long-term stability than CZA individuals [87]. On the contrary, Palgunadi et al. [88] did not found much difference in the catalytic activity over Mn modified CZA. The addition of Pd into the CZA/γ-Al_2O_3 hybrid catalyst induces hydrogen spillover from metallic Pd to metallic Cu [28b]. This reduces the oxidation of active Cu by CO_2 and increases the stability of active Cu. Increasing CO_2 concentration in syngas reduces the activity of the physically mixed catalyst (Table 5). Besides, Zhang et al. [89] recently reported a good activity and stability for hybrid catalysts comprising a Cu-based methanol synthesis catalyst supported on carbon nanotubes, mixed with γ-Al_2O_3 and HZSM-5 for methanol/DME synthesis from CO/CO_2 hydrogenation.

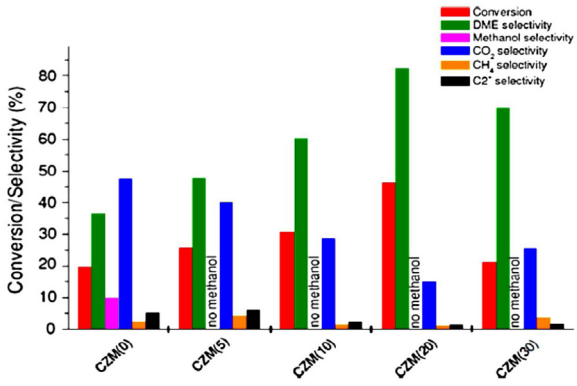

Fig. 11. The effect of MgO content on hybrid Cu/ZnO/MgO(CZM)–γ-Al_2O_3 catalyzed conversion of CO and selectivity of the products. Reaction conditions: 30 bar, 260 °C, 2000 mL/(g_{cat} h), and H_2/CO ratio of 1.5 [27].

Asthana et al. [27] have shown that MgO can be an interesting replacement for Al^{3+} because of the similar charge of Mg^{2+} and Zn^{2+}, and the only 2% smaller ionic radius of Mg^{2+} than of Cu^{2+}. Thus, more Cu dispersion per unit weight of catalyst can be expected in the presence of MgO. It is noted from the catalysis results that among all the catalysts containing the same amount of γ-Al_2O_3, only the CZM(0)-catalyzed reaction, where no MgO was there, showed unconverted methanol in the product (Fig. 11). As methanol was completely converted in the presence of MgO, the role of MgO in enhancing the dehydration activity of γ-Al_2O_3 was evident. The small quantities of basic sites are required along with Lewis acidic γ-Al_2O_3 for methanol dehydration to DME. Mao et al. [91] have also reported the importance of basic sites in the catalyst during methanol dehydration to DME.

3.1.4. *Cu/ZnO with γ-Al_2O_3 catalyst*

Few reports are available on STD process without addition of alumina in MSC. In this respect, Kim et al. [65] and Baek et al. [92] studied the effect of copper precursors and confirmed that the catalyst prepared by the copper acetate (CZA(A)) precursor having more acidic sites and a suitable surface area of metallic copper and thus higher reaction rate than the catalyst prepared by the copper nitrate (CZA(N)) and copper chloride (CZA(C)) precursors. Allahyari et al. [93] also showed that a copper acetate precursor exhibited better reactivity in the presence of CZA/HZSM-5. It was also believed that

Table 4
Modified Cu/ZnO/Al_2O_3 with γ-Al_2O_3 catalyst for STD reaction.

MSC	Reaction conditions and catalytic activity							Ref.
	H_2:CO ratio	T (°C)	P (bar)	SV	X_{CO} (%)	Y_{DME} (%)	S_{DME} (%)	
Ga/CZA	2:1	250	50	4000 mL/gcat/h	63.9	33.9	53.1	[84]
Zr/CZA	2:1	250	50	4000 mL/gcat/h	72.3	40.3	55.7	[84]
Y/CZA	1.5:1	280	41	6000/h	70.0	47.7	–	[85]
Zr/CZA	~2:1	270	50	1500/h	79.3	–	85.8	[86]
Mn/CZA	2:1	260	50	2.0 L/g cat h	66.7	51.0	76.5	[87]
Mn/CZA	1.5:1	270	41	–	85.0	58.0	–	[88]
Pd/CZA	2.4:1	220	40	15000 mL/gcat/h	60.0	–	59.0	[28b]

Table 5
Effect of CO_2 contents in feed gas for CO and H_2 conversions as well as DME selectivity and yield over Pd modified CZA/γ-Al_2O_3 hybrid catalyst [28b].

CO_2 content (vol%)	$H_2/CO/CO_2/N_2$ (vol%)	CO conversion (%)	H_2 conversion (%)	DME selectivity (%)	DME yield (g/(g_{cat}·h)
0	64/32/0/4	63	34	60	2.12
3	63/30/3/4	63	36	59	2.06
5	61/30/5/4	56	34	62	1.93
10	61/25/10/4	55	29	62	1.56
16	48/32/16/4	39	35	66	1.43
32	64/0/32/4	–	12	10	0.13

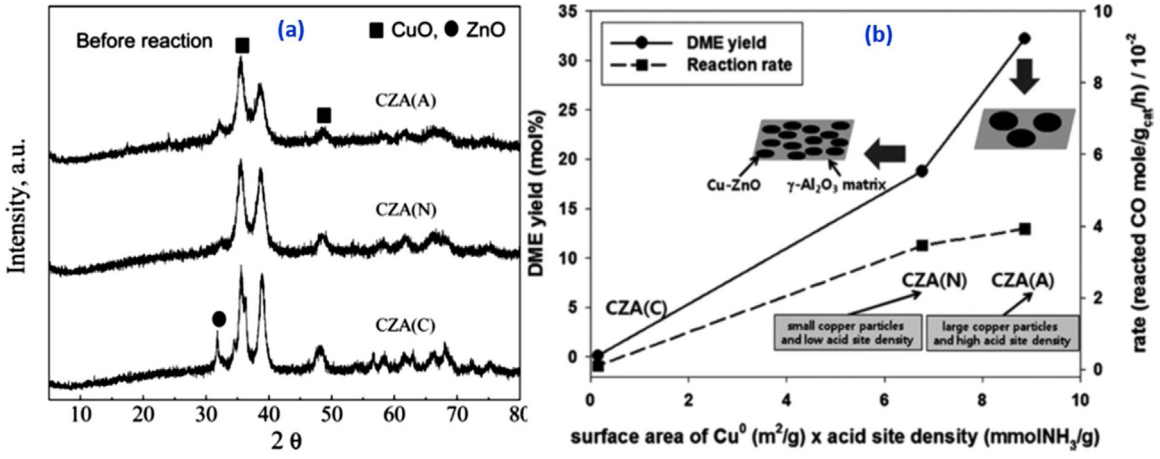

Fig. 12. (a) PXRD patterns on the fresh CZA bifunctional catalysts and (b) correlation on the reaction rate and the DME yield to the copper surface area multiplied with the amount of acidic sites [CZA, where C, Z, and A represent CuO, ZnO, and γ-Al_2O_3, respectively and copper precursors, *i.e.* copper acetate (A), nitrate (N), and chloride (C)] [92].

the reactivity of catalyst was related to the crystallinity of metal nanoparticles on the hybrid catalysts [65]. The crystallinities of the CuO and ZnO in the CZA(N) and CZA(C) were found to be higher, which indicates that the much larger CuO and ZnO crystallites can be formed and a higher reactivity can be expected on the CZA(A) having smaller crystallite sizes (Fig. 12a). The reaction rate and DME yield showed an excellent correlation with the surface area of Cu^0 multiplied with the amount of acid site density [92,94], as shown in Fig. 12b.

More recently, colloidal catalysts offer a broad range of possibilities to tune or control the physico-chemical properties such as the particle size, solubility and functionality [95]. This method also ensured a high proportion of Cu/ZnOx interface along with the intimate contact of the nanoparticulate methanol active component with the dehydration component, enabled the individual optimization and balancing of the two active functionalities in the bifunctional catalyst [47a]. In this colloidal chemistry method, mixing copper(II) precursors and diethyl zinc, under the appropriate conditions, leads to the formation of a pre-catalyst colloid consisting of Cu^o nanoparticles and intermediates of diethyl zinc and a heteroleptic alkyl zinc carboxylate complex species [47,96]. The precatalyst colloid of Cu^o/ZnO nanoparticle solution was subsequently supported on conventional dehydration catalyst like γ-Al_2O_3 (Fig. 13).

In this regard, Gentzen et al. [47a] prepared hybrid catalysts by dispersing the sieved fraction of γ-Al_2O_3 in the suspension of the Cu and ZnO nanoparticles, which, after calcination, leads to immobilized Cu and ZnO nanoparticles. Although the initial catalytic tests revealed a high DME selectivity over nanoparticle derived hybrid catalysts, the same reaction rates and long-term stability did not maintained during 2.6 h time on stream. When the catalysts were isolated after the catalytic performance, the XRD measurements revealed an increase in the crystallite size from 7 nm to 16 nm of the metallic Cu^o particles and a sintering behaviour, which was believed for the deactivation of nanoparticle catalysts. On the contrary, a low Cu^o ripening rate was observed by García-Trenco et al. [47b] even after an exposure of CuZnO@st/γAl hybrid catalyst to the reaction conditions for 20 h time on stream. They claimed that the low sintering rate of the catalyst particles can be attributed to the presence of the stearate ligand which may help for stabilising the nanoparticles. Evidence for this hypothesis is provided by a control experiment performed using copper(II) bis(acetate) to prepare the colloidal Cu/ZnO nanoparticles; the shorter ligand (*i.e.* acetate) is not expected to provide steric stabilisation to prevent the ripening of the Cu^0 and ZnO nanoparticles. This hypothesis is

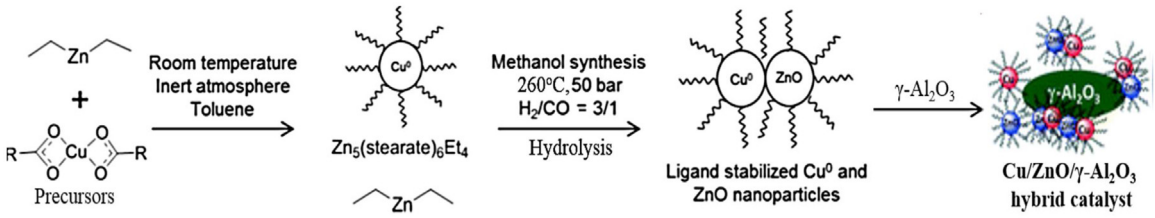

Fig. 13. Representation of the formation of the ligand-stabilized Cu and ZnO nanoparticles from diethyl zinc and bis(stearate)copper(II) precursor followed by mixing of γ-Al_2O_3 to pre-formed Cu and ZnO nanoparticles [modified form from Ref. [96]].

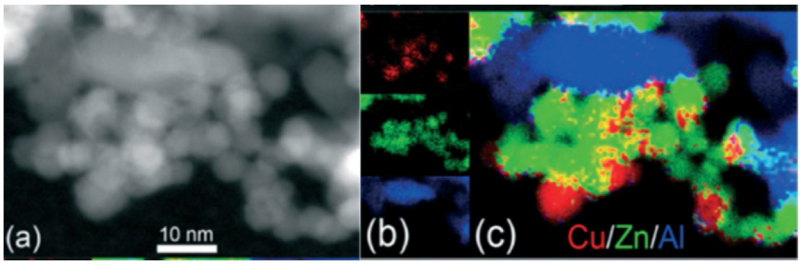

Fig. 14. (a) Representative ADF-STEM image of the used catalysis sample CuZnO@st/γAl with a Cu/Zn ratio of 1 and CuZnO/γ-Al_2O_3 mass ratio of 1/2. (b) Cu (red), Zn (green) and Al (blue) EDX maps. (c) Overlay of (a) and (b) showing the location of Cu, Zn and Al [47b]. (For interpretation of the references to colour in this figure legend, the reader is referred to the web version of this article.)

also well matched for the deactivation behaviour of immobilised colloidal Cu/ZnO nanoparticles onto γ-Al_2O_3, where the acetate ligand (copper(II) bis(acetate) used as Cu precursor) was removed by air calcination [47a]. In the hybrid catalysts, a detailed understanding of the active species and their related contact helps to improve the fundamentals of catalysis and to optimize existing catalyst formulations or develop completely new ones. In this context, García-Trenco et al. [47b] used angular dark field scanning TEM (ADF-STEM) images revealed intimate mixed agglomerates of Cu and Zn-containing nanoparticles along with larger γ-Al_2O_3 particles (Fig. 14). These images confirm that both catalytic components are in very close proximity in the reaction medium, and hence low ripening rate of the Cu^0 and the formed methanol can be quickly converted to DME, during the reaction. This seems that alumina might not be the vital component in MSC if copper is well dispersed on supports.

CZA catalyst itself can act as a hybrid catalyst if the alumina content (>50 wt% with respective to CuO/ZnO) and calcination temperature (~500 °C) be higher to produce suitable amount of γ-Al_2O_3 as a dehydration catalyst [45,68]. Therefore, CZA slurry catalyst containing AlOOH binder, where the gel-type CZA slurry dispersed in paraffin for transferring it into a slurry reactor for the catalyst preparation, is quite effective catalytic system for the single-step synthesis of DME from syngas since the boehmite (AlOOH) also plays an important role in methanol dehydration activity [97].

3.1.5. *Mesoporous Cu/γ-Al_2O_3 catalyst*

Syntheses and applications of mesoporous materials having an ordered mesopore structure with a large specific surface area have been widely reported, since the ordered mesoporous materials have superior characteristics such an easy mass transfer and a high dispersion of active metals [98–100]. Therefore, a great number of bifunctional (or hybrid) catalytic systems containing metallic sites for carbon oxides hydrogenation as well as acid sites for a successive dehydration of alcohols to ethers have been extensively investigated by using the mesoporous materials, especially for the direct synthesis of DME from syngas [60,98,101–103]. Compared to the conventional wet impregnation method or physical mixing, the mesoporous alumina supported metals by one-pot method were reported to have high-quality mesostructures that exhibit strong metal-support interactions and a homogeneous distribution of active sites [101,104].

Recently, Jiang et al. [101] used a one-pot solvent evaporation induced self-assembly (EISA) method for the synthesis of mesoporous Cu–γ-Al_2O_3. From the scanning TEM (STEM), both ordered and worm-like mesoporous regions are observed in the bifunctional catalyst (Fig. 15). The sample 5Cu–Al-800 (where, 5 = mol% of Cu precursor and 800 = calcination temperature used) after reduction at 650 °C, small Cu particles (light white dots) with the size of around 6 nm were detected that are well distributed over the entire alumina network in the ordered (Fig. 15a and 15c) as well as worm-like (Fig. 15b and d) mesoporous structures. The 5Cu–Al-800 catalyst displayed an excellent CO conversion of 72% and DME selectivity of 69% at 50 bar and 310 °C. Although the catalytic activity of mesoporous Cu–γ-Al_2O_3 was superior, the synthesis of the exclusively ordered phase of alumina with the presence of copper species was not well investigated till now.

In order to overcome the above problems, our group studied a spatial confinement effect of copper nanoparticles in an ordered mesoporous γ-Al_2O_3 [98]. EISA method was adopted for synthesis of highly ordered mesoporous γ-Al_2O_3 which subsequently impregnated by copper nitrate. The ordered mesopore structures of Al_2O_3 were effective to suppress the aggregation of copper nanoparticles even under reductive CO hydrogenation conditions through the spatial confinement effect of the ordered mesopores of Al_2O_3 as well as the formation of strongly interacted copper nanoparticles within the mesoporous Al_2O_3 surfaces by partial formation of the interfacial thermally stable spinel copper aluminate ($CuAl_2O_4$) species. This $CuAl_2O_4$ species helps to generate new acid sites for dehydration of methanol intermediate to DME. The highly dispersed copper nanoparticles (~5 nm) with strong interactions on the abundant acid sites of the ordered mesoporous Al_2O_3 largely enhanced the catalyst stability and DME selectivity as well. The proposed spatial confinement effects inside of the mesoporous Al_2O_3 was verified by TEM analyses of the Cu/mesoAl(HT) before (Fig. 16(A)) and after reaction for 40 h (Fig. 16(B)). The size of copper crystallites was not significantly altered even after reaction for 40 h as shown in Fig. 16(B).

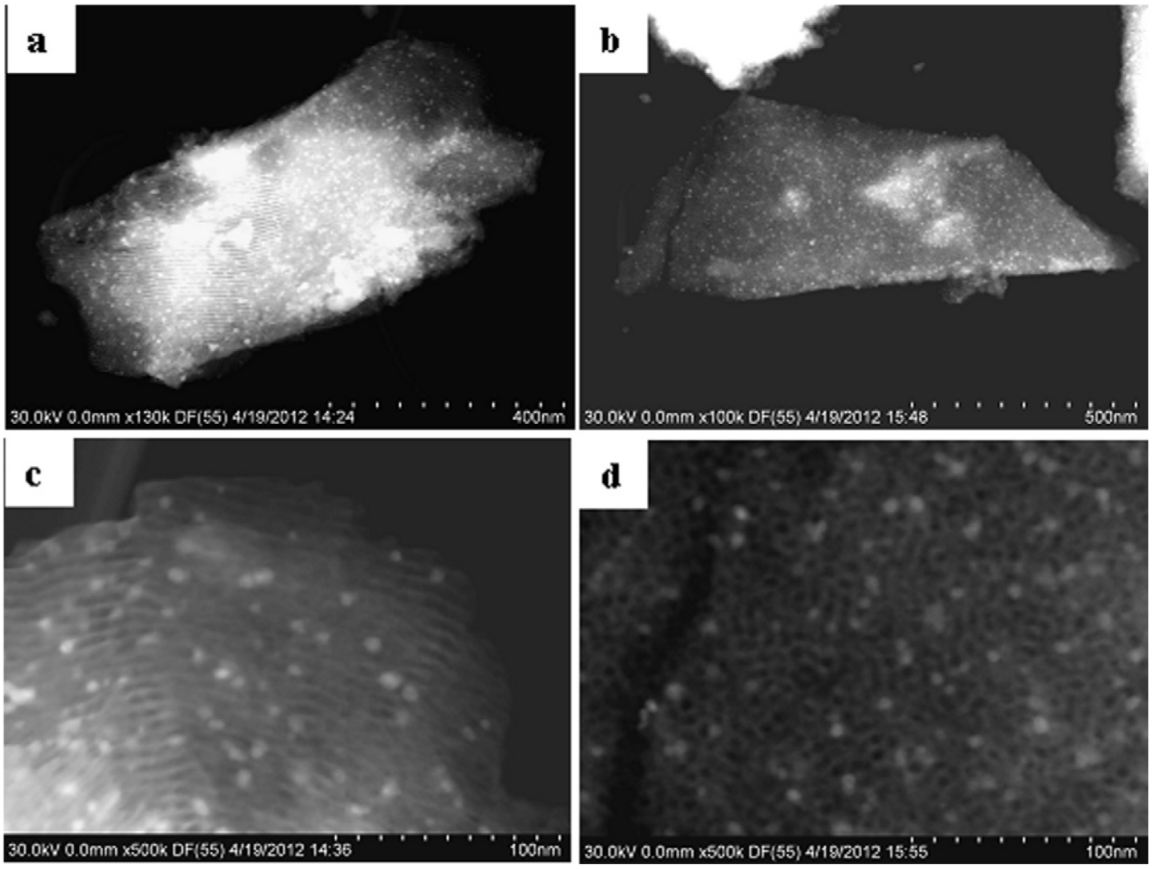

Fig. 15. STEM dark-field images of the sample 5Cu–Al-800 reduced at 650 °C for 4 h. (a) and (c) ordered; (b) and (d) worm-like mesoporous structure (light white dots are Cu particles) [101].

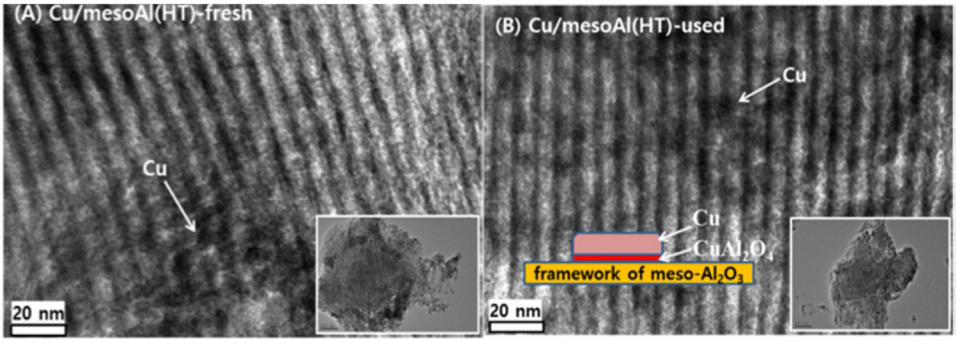

Fig. 16. HR-TEM and TEM (inset) images of the (A) fresh and (B) used Cu/mesoAl(HT) [98].

Ordered mesoporous copper incorporated Al_2O_3 with high Cu dispersion were prepared using a facile solution combustion synthesis method by Wang et al. [102]. The ordered mesoporous structure and copper was homogenously dispersed on Al_2O_3 shows good catalytic activity and excellent stability during 56 h on stream. Although many authors reported on the importance of the ZnO for methanol synthesis, the above results suggest that the active ZnO-free Cu-based catalysts can also achieve the high catalytic activity in the STD reaction.

3.2. Hydrogenation of CO by Cu-based MSC and zeolites as MDC

3.2.1. CZA with pure and modified ZSM-5 catalysts

It is widely accepted that the alumina-based catalysts, either pure or modified, are relatively sensitive toward deactivation by competitive adsorption of water and also by coke formation. Furthermore, as the temperature required in STD on γ-Al_2O_3 dehydration catalysts is typically above the optimum temperature required in the methanol synthesis step and thus the Cu-based component is more prone to deactivate, typically by sintering, and the overall activity of the bifunctional catalyst becomes lowered [72]. As compared to traditional γ-Al_2O_3, the zeolite based catalysts have several advantages such as tunable acidity and better stability [46,105]. Generally zeolites due to their hydrophobic nature show higher catalytic activity than γ-Al_2O_3 even at lower reaction temperatures where the methanol synthesis step (Eq. (1)) becomes thermodynamically more favored [9,61,106,107]. Proton and non-proton form of zeolites such as ZSM-5, ferrierite, mordenite and zeolite-Y are widely studied solid acid catalysts for STD reaction. Among these, ZSM-5 based catalysts are of particular interest by

Table 6
$Cu/ZnO/Al_2O_3$ with pure and modified ZSM-5 catalysts for STD reaction.

Catalyst	Preparation method	Reaction conditions and catalytic activity							Ref.
		H_2:CO ratio	T (°C)	P (bar)	SV	X_{CO} (%)	Y_{DME} (%)	S_{DME} (%)	
CZA/HZSM-5	Sedimentation	2:1	270	40	1500/h	89.4	–	87.2	[30b]
CZA/ZSM-5	PM	2:1	225	40	15000 mL/gcat.h	57.1	–	93.0	[32]
CZA/ZSM-5	PM	2:1	260	50	1500 mL/gcat.h	87.8	–	65.9	[43b]
CZA/HZSM-5	PM		260	20	3600 cm^3/gcat h	82.2	–	71.4	[46]
CZA/HZSM-5	AM	2:1	260	20	2400 mL/gcat h	–	100	–	[61]
CZA/HZSM-5	PM	1:1	250	50	–	~30	–	~70	[108]
CZA/HZSM-5	PM	1.2:1		30	1300 L/(kg. h)	~77	–	~76	[109]
CZA/HZSM-5	PM	2:1	260	30	–	69.2	–	64.8	[111]
CZA/ZSM-5	kneading	2:1	260	20	3600 mL/gcat.h	~64	–	66.1	[113]
CZA/SiO_2-ZSM-5	kneading					~68	–	68.4	[113]
CZA/HZSM-5	PM	2.2:1	260	40	1.7 L/gcat.h	89.4	56.9	63.7	[114]
-/ZSM-5	PM	3:1	280	38	5000/h	80.0	–	60.2	[121]
CZA/HZSM-5	CP deposition	1:1	260	40	3000 mL/gcat/h	48.5	–	97.0	[122]
CZA/HZSM-5	PM	2:1	240	50	1000/h	90.0	70.0	78.0	[123]
CZA/HZSM-5	CP	2:1	275	40	600 cm^3/gr.h	60.0	46.1	–	[124]
CZA/HZSM-5	PM	2:1	240	50	1100 mLn/(g-cat h)	83.5	51.1	–	[125]
CZA/HZSM-5	PM	1:1	240	30	3000 mL/gcat·h	~66	–	63.0	[126]
CZA/HZSM-5	Combustion	2:1	300	40	600 cm^3/g h	39.0	29.0	–	[127]
CZA/HZSM-5	Ultrasound	2:1	275	40	600 cm^3/gr.h	50.5	–	55.0	[128]
CZA/NaZSM-5	AM	1.5:1	280	42	6000 mL/gcat h	45.5	27.8	~65	[105]
CZA/NaHZSM-5	Slurry	2:1	275	40	–	~100	78.0	80.0	[129]
CZA/Na and CoZSM-5	Mixing the pre-pelletized components	2.2:1	260	40	1700 mLsyngas/(gcat h)	~90	–	60–65	[115]
CZA/MgO-ZSM-5	PM	2.2:1	260	40	1500 mL h^{-1} g^{-1}	96	–	64.0	[91]
CZA/CaO— HZSM-5	PM	2.2:1	260	40	1500 mL/(h.gcat)	94.1	–	67.5	[130]
CZA/CaO— HZSM-5	PM	1.2:1	270	30	1300 L/(kg h)	~73	–	~77	[131]
CZA/Sb_2O_5— HZSM-5	AM	2.2:1	260	40	1500 mL/(h.gcat)	95	65.6	69	[132]
CZA/Zr-ZSM-5	Slurry	~1:1	250	40	5550 mL/h/gcat	23.3	–	27.9	[133]
CZA/HFeAl-ZSM-5	PM	2:1	260	40	1500 mL/(h.gcat)	95.5	–	67.1	[134]
CZA/Na_2CO_3+ HCHO treated HZSM-5	PM	1.2: 1	260	54.4	4500 mL/h/gcat	45.2	30.2	66.8	[80]

The abbreviations represent PM for physical mixing; AM for admixed; and CP for coprecipitation.

many researchers (Table 6) as the medium size of its pores (Table 1) prevents extensive coking without severely hindering the diffusion of the molecules involved in the DME synthesis.

Although there is a general agreement in the researcher that the acidity of the zeolite is the most important parameter to determine its catalytic performance for the STD reaction [108–129], inconsistencies appear regarding the required amount and strength of the acid sites in the zeolite dehydration component [72]. In the case of γ-Al_2O_3, methanol dehydration can take place only on Lewis acid–base pairs generated on the γ-Al_2O_3 surfaces, as shown in Fig. 8. However, different mechanism involves in the case of zeolites where a Brønsted acid (H^+) or both Brønsted acid and its adjacent Lewis base sites (O^{2-}) have been proposed for the DME formation from methanol dehydration. The nature and strength of the acid sites of zeolite surfaces, and the interaction of methanol with these sites determine the reaction path, yield and selectivity [107]. The STD activity arises from the fact that in some of the studies the overall rate of STD reaction is controlled by the syngas-to-methanol step, while in others the rate-determining step is that of the methanol dehydration reaction [72]. In the first case, the presence of strong acid sites in the MDC may not result in noticeable changes in CO conversion but it mainly affects DME selectivity [105,108], whereas in the latter case, both the CO conversion and the selectivity for DME were greatly affected when the acidity of the acidic component was not strong enough to convert effectively the originally produced methanol to DME [78,105]. However, it is possible to draw some conclusions from the results published. For example, Ramos et al. [108] compared the catalytic activity of different acidic components namely porous Al_2O_3 (Alumina-C) and non-porous Al_2O_3 (Alumina-D), HZSM-5, sulfated zirconia (S-ZrO_2) and tungstated zirconia (W/ZrO_2) which were physically mixed with commercial methanol catalyst (ACZ). The results from Fig. 17 show that all catalysts were indeed active for both methanol dehydration and STD reaction, though they have differences in Lewis and Brønsted acid sites concentration. However, comparing the direct synthesis of STD activities over the physically mixed catalysts (Fig. 17(b)) with the solid acid catalysts performances shown in Fig. 17(a), it can be seen that they do not follow the same order. HZSM-5 and S-ZrO_2 catalysts after mixed with MSC (*i.e.* ACZ) achieved the best catalytic activities for STD, although HZSM-5 exhibited the highest Brønsted acidity and methanol dehydration rate than S-ZrO_2 (Fig. 17). This result allowing the conclusion that the overall reaction rate can be determined by the methanol synthesis step (Eq. (1)) rather than the methanol dehydration step (Eq. (2)). On the contrary, other lower acidic materials like Alumina-C, D and W/ZrO_2 prepared with ACZ inferred that the methanol dehydration rate controls (Eq. (2)) the activity of direct DME synthesis. A similar conclusion was drawn for the CZA/HZSM-5 hybrid catalyst prepared with Si/Al ratio of 38 which has an appropriate amount of Lewis to Brønsted acid sites as compared to other Si/Al ratio of 25, 50 and 150 [109].

It is well known that the Brønsted acid sites of zeolites are closely related to the tetrahedral aluminum ions in the framework of the zeolites [91]. Hence, the acidity can be tuned by varying Si/Al ratio which affecting its catalytic activities and hydrothermal stability particularly. Kim et al. [105] had investigated NaZSM-5 and HZSM-5 with three different Si/Al ratios of 30, 50, 100 for methanol dehydration and STD conversion. They found that the NaZSM-5 was much less active than HZSM-5 for methanol dehydration, though their Si/Al ratio of 30 was same, which suggesting that both Brønsted and Lewis (related to Na^+) acid sites may be active for methanol dehydration, though the Brønsted acid sites would display a much higher

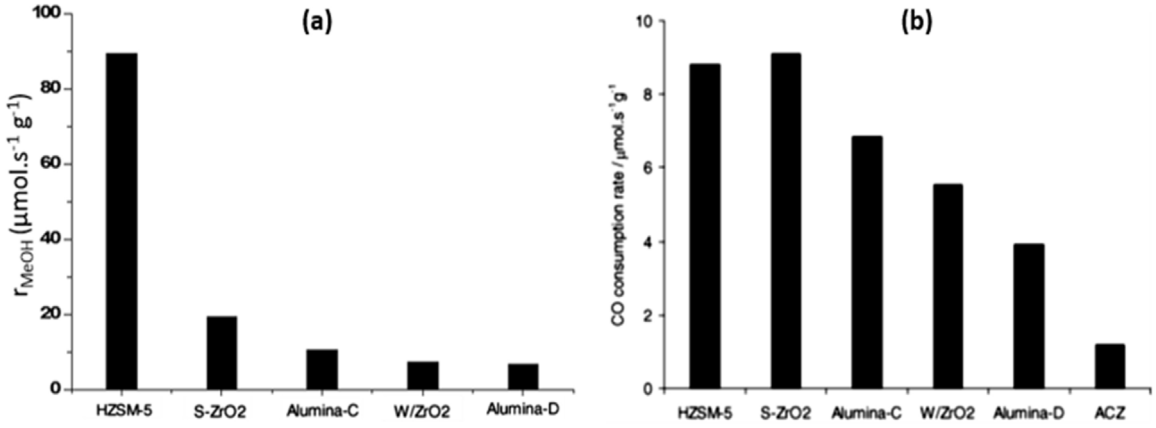

Fig. 17. (a) Methanol dehydration rate over different solid acid catalysts and (b) CO consumption rate over the physically mixed catalysts of ACZ and solid acid catalysts [108].

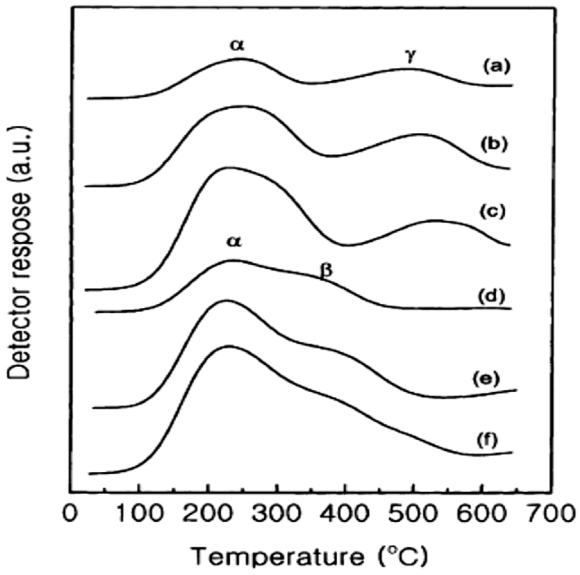

Fig. 18. NH_3-TPD spectra of ZSM-5 catalysts different Si/Al ratios: (a) HZSM-5(100); (b) HZSM-5(50); (c) HZSM-5(30); (d) NaZSM-5(100); (e) NaZSM-5(50); (f) NaZSM-5(30) {α = weak acidity; β = moderate acidity; γ = strong acidity} [105].

intrinsic activity. The strong acid sites of HZSM-5(γ) increased with decrease in the Si/Al ratios from 30 to 100, leading to a change in rate of MeOH dehydration as compared to NaZSM-5, which was related to a concomitant weakening in the acid strength, according to NH_3-TPD data (Fig. 18). However, they did not find any significant changes in CO conversion and DME selectivity with the acidity of the ZSM-5 when the overall STD process is governed by the methanol synthesis step. In contrast, the changes in both CO conversion and DME selectivity were noticed over HY zeolite supported Cu–Mn–Zn catalysts when the acidity of HY zeolite was modified via ion-exchange with transition (Fe, Co, Ni, Cr and Zr) [110] and rare earth (La, Ce, Pr, Nd, Sm and Eu) [73] metals as well.

In parallel, the influence of the type of zeolites (HZSM-5 and H-Y) and their Si/Al ratio in the CZA–zeolite was investigated by Xia et al. [43b]. Comparing the three HZSM-5 zeolites with different Si/Al ratio (30, 80 and 280), it can be found that the lowest CO conversion (44.6%) but highest DME selectivity (70.4%) was obtained over HZSM-5(280). On the other hand, the higher CO conversion (87.8%) and comparable DME selectivity (65.9%) was observed for HZSM-5(30) as the high surface acidity is responsible for the high CO conversion during STD process. However, the catalytic activity of H-form Y zeolite does not depend on the Si/Al ratio, indicating that this likely originates from the lower acidic strengths of the Brønsted acid sites. In another study, Wang et al. [111] varied Si/Al ratio of 50 and 300, and found the lower Si/Al ratio was best to obtain good activity of STD catalyst after mixing of CZA and HZSM-5. The influence of the Si/Al ratio was also described by Mao et al. [112], but with an HMCM-22 zeolite displayed that at higher Si/Al ratios, the proportion of strong acid sites decreases which is beneficial to the increase of the DME selectivity. The above experimental results concluded that the overall DME synthesis rate can be determined by the relative ratio of methanol synthesis and methanol dehydration components along with reaction conditions.

Ordomsky research group investigated a series of hybrid CZA/ZSM-5 catalysts prepared by kneading with different Si/Al ratio and crystallite size [46,113]. The results revealed that the initial performance of the hybrid catalysts depend on both ZSM-5 Si/Al ratio and particle sizes. In more details, higher concentration of Brønsted acid sites and smaller zeolite crystallite sizes favor higher DME selectivity [113]. However, the activity of the hybrid catalysts gradually decreased with time on stream (TOS) due to simultaneous copper sintering, copper oxidation and ion exchange of the acidic proton of ZSM-5 with Cu ion from CZA catalyst causes the deactivation of the ZSM-5 in hybrid catalyst (Fig. 19). The result also indicated that the copper sintering, and copper migration leading to the decrease in the concentration of zeolite Brønsted acid sites could be major reasons for deactivation of the hybrid catalysts. García-Trenco et al. [114] also mentioned a similar phenomenon of migration of Cu^{2+} ions (possibly Zn species as well) to proton-exchange in HZSM-5, cause an increase in the Lewis acidity. The possible Cu cation migration was unambiguously evidenced through the analysis of electron paramagnetic resonance (EPR) spectroscopy. For preventing copper sintering and migration, selective neutralization of Brønsted acid sites on the outer zeolite surfaces were done using silylation (*i.e.* TEOS) which results in the better catalyst stability (Fig. 19) and slightly higher selectivity towards DME [113]. The results demonstrated that, besides zeolite acidity, the zeolite crystallite size and crystallite aggregation can also strongly affect the rate of direct DME synthesis. The catalyst containing smaller individual zeolite crystallites (60–100 nm) was superior in terms of the enhanced transport of methanol from the Cu surfaces to the acid sites of zeolites than their counterparts with the inter-grown agglomerates. Moreover, the zeolite crystallite sizes have more significant effects of the reaction rate than the concentration of Brönsted acid sites [46].

It is also believed that there is a possible detrimental interaction within the components due to a partial exchange of the zeolite pro-

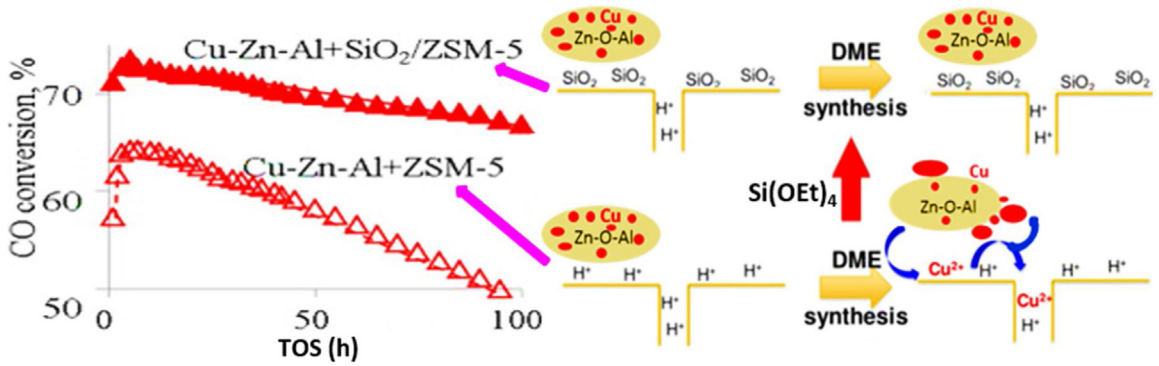

Fig. 19. CO conversion with TOS during DME synthesis over CZA-zeolite with before (Cu-Zn-Al + ZSM-5) and after (Cu-Zn-Al + SiO_2/ZSM-5) silylation, and schematic representation of Cu migration leading simultaneously to ion exchange with acidic proton of the ZSM-5 zeolite and Cu sintering [113].

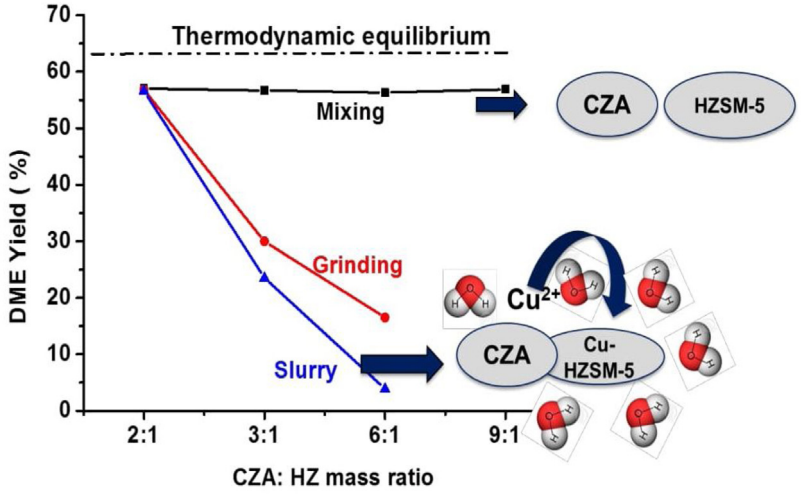

Fig. 20. DME yield with respective to CZA:HZ ratios over hybrid catalysts prepared by mixing, grinding and slurrying methods [114].

tons by Cu^{2+} species, which caused to decrease a Brønsted acidity. In order to confirm such detrimental interaction between the components in CZA/HZSM-5 hybrid catalyst, García-Trenco et al. [114] conducted a thorough study addressing the influence of the catalysts mixing methods such as grinding of catalyst powders prior to pelletizing, slurrying of two solid components in water (drying and then pelletizing) and physical mixture of pre-pelletized components. They achieved the best results by mixing the catalyst components when already pelletized. Grinding or slurrying methods resulted in drastic reduction in the amount of Brønsted acid sites increased the possibility of interactions and reduced the efficiency of the final STD catalyst. Fig. 20 shows that lower DME yields were attained with increasing CZA/HZSM-5 (CZA:HZ) ratios for the catalysts prepared by grinding and slurry methods as compared to that obtained by the mixing of individual pellets which holds the individual components unchanged during the synthesis process. The inter-cation exchange effect was seen to be more pronounced for the hybrid catalysts prepared by the slurry approach (Fig. 20). Takeguchi et al. [75] concluded a similar viewpoint for CZA–Cr_2O_3–Ga_2O/silica–alumina hybrid catalyst prepared by mixing the pre-pelletized components is more active for the STD reaction than the same catalyst obtained by milling the two component powders prior to pelletizing process.

García-Trenco et al. [114–117] have widely studied the performance of the hybrid CZA/zeolite catalysts, including the effect of zeolite pore structures, surface-aluminum species, and acidity along with the deactivation behaviors. In this context, they used 10 member-ring 2- and 3-dimensional zeolite structures namely ZSM-5, FER, IM-5, TNU-9, MCM-22 and ITQ-2 as MDC for the STD process [116]. The authors attributed a strong correlation between the zeolite external surface area and the loss of dehydration activity for the hybrid catalysts containing medium pore zeolites. These results confirm that the interactions between zeolitic Al species and Cu sites which depends on the availability of acid sites in the exterior of the zeolite crystallites [116,117]. In another extensive study, Montesano et al. [118] reported that DME selectivity, stability and formation of hydrocarbons were found to depend on the topology of the zeolite used namely theta-1, ZSM-23, ferrierite, ZSM-5 and mordenite. For example, DME obtained exclusively over ferrierite and theta-1 which were found to be the most stable catalysts. The lower stability of ZSM-23, due to its larger crystallite size (0.52 nm × 0.45 nm), imposes the diffusion constraints which are favor the formation and accumulation of C_{4+} hydrocarbons. On the other hand, the mordenite and ZSM-5 are relatively wide pores (Table 1) accommodating oligomers and aromatics and thus showing a significant deactivation.

A lack of agreement is also evidenced from the reported literature on the direct DME synthesis with respect to the necessities in terms of the type of acid strength and acid sites to effectively produce DME. Quite often the contribution of different type of acid strengths for the dehydration catalysts was exclusively characterized by using the NH_3-TPD technique which obviously not able to discriminate between Brønsted and Lewis acid sites [115]. Many authors concluded that the acid sites of weak and/or moderate

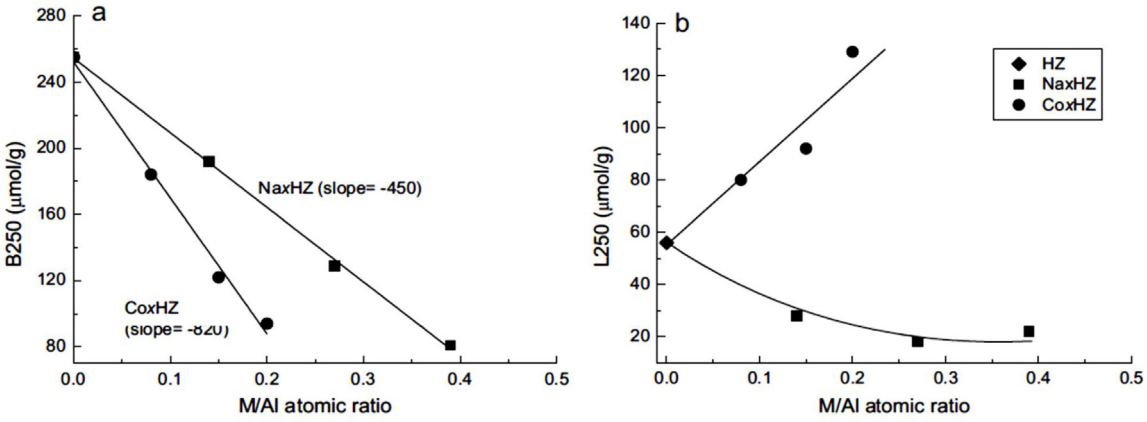

Fig. 21. Correlations between the acid properties and the atomic M/Al ratio (M = Na, Co) for partially exchanged ZSM-5 samples: (a) total amount of Brønsted acid sites (B250) and (b) total amount of Lewis acid sites (L250) [115].

strength (deduced typically from NH_3-TPD) are the most desirable for DME selectivity [50,71,78,61,91,94,119], although Kim et al. [105] associated the dehydration activity of zeolites to the presence of very strong acid sites (Fig. 18). Concerning the acid sites, strong Brønsted acid sites in zeolites (deduced from pyridine IR) favor the conversion of DME to hydrocarbons [39b,75,119]. However, Xia et al. [120] claimed that extra lattice Al species, which is related to the Lewis acidity in zeolites, can promote the formation of hydrocarbons during the STD reaction. On the other hand, Mao et *al.* [91] did not find any direct relationship between the activity for methanol dehydration and the nature of the acid sites on HZSM-5 modified by basic MgO (decreased Brønsted and increased Lewis acidity by doping of 5 wt%) and proposed a mechanism for DME formation involving both acidic and basic sites.

To gain more insights into the influence of the acid property of the dehydration catalyst, García-Trenco et al. [115] prepared a series of hybrid CZA/HZSM-5 catalysts in which the zeolite's acid site, density, and strength was systematically varied by submitting HZSM-5 to mild acid treatment (HZ) and partial exchange of H^+ by Na^+ (Na*x*HZ) and Co^{2+} cations (Co*x*HZ). The acid properties of the hybrid catalysts were measured by applying both NH_3-TPD and FT-IR-pyridine techniques. For both the Na*x*HZ and Co*x*HZ (where *x* is cation content) series the amount of total Brønsted acid sites (after desorbing pyridine at 250 °C, B250) decreased with increasing the cation contents. In fact, a good linear correlation between B250 and the atomic M/Al ratio becomes apparent in Fig. 21a. On the other hand, the change in Lewis acidity showed different trends depending on the nature of the exchange cations. The density of Lewis acid sites (L250) decreased with Na^+ while the reverse trend was observed upon Co^{2+} cations (Fig. 21b). Indeed, the FT-IR-pyridine spectra on the Co*x*HZ hybrid catalysts confirmed that the Co^{2+} species located at the ion-exchanged positions on the HZSM-5 generated Lewis acid sites with lower acid strengths than those of the EFAL species (generated from the extra-framework Al species). This study concluded that the zeolite dehydration activity was mostly determined by the density of strong Brønsted acid sites with a small contribution of EFAL-related Lewis acid sites for the STD process when using the CZA/ZSM-5 hybrid catalysts with a low zeolite concentration.

Modification of the ZSM-5 with basic oxides namely MgO, CaO, ZnO [130,131], and Sb_2O_5 [132], and by impregnation with solutions containing certain transition metals such as Zr [133] and Fe [134] leads to the restructuring of the zeolite acid strength toward weaker sites with the consequent improvement in the DME selectivity and stability (Table 6).

3.2.2. Pure and modified CZA/ferrierite catalysts

As mentioned before, the deactivation of the zeolites during the STD reaction is a shape-related phenomenon determined by the pore structure and the crystallite size of the zeolites. Pure or modified ferrierite takes attention from many researchers, including our group, because of its superior catalytic performance related to the higher selectivity towards DME (Table 7) and the superior stability in comparison to other zeolite structures. Montesano et al. [118] systematically studied about zeolite topology and concluded ferrierite (FER) prevents the formation of hydrocarbons, possibly by providing a preferential path for the diffusion of small reactants and products (*i.e.* methanol and dimethyl ether). In parallel, Prasad et al. [11a] reported higher stability and selectivity to DME over the CZA/HFER bifunctional catalysts compared to HZSM-5, NaY and HY. Kang et al. [133] investigated the STD process from biomass based synthesis gas over CZA/Zr modified composite catalysts. They obtained a maximum CO conversion (49.0%) and DME selectivity (58.2%) with Zr modified FER which has low copper surface area and an appropriate acid sites of required strength for methanol dehydration as compared to ZSM-5 and Y zeolites. Flores et al. [135] observed that the CO conversion was more pronounced in the CZAZr/HFER sample in comparison with undoped Zr on CZA/HFER sample. The effect of Zr content on CZA/FER catalysts was also studied by our research group [94,136]. According to results, 3 wt% Zr on FER showed the best catalytic performance, attributed to the facile reducibility of copper species (co-presence of Cu^+–Cu^0). The nature of precipitant used for CZA/Zr-FER synthesis was also influenced on DME yield. For instance, the best DME yield was obtained over the catalyst precipitated by using $(NH_4)_2CO_3$ than Na_2CO_3 and K_2CO_3 [137].

In our subsequent papers, alumina modified FER catalysts was investigated to elucidate the effects of acidic sites and copper surface area to the intrinsic activity. The main role of Al_2O_3 on HFER was found to reduce selectively strong acidic sites with an enhanced interaction of copper particles, which resulted in a higher CO conversion of 61.8% and yield of DME (45.2%) (Table 7) [138]. We have also correlate the reaction rate and intrinsic activity (TOF) of CZA/Al-FER by combining the results of CZA/Zr-FER with respect to the product values of the amount of acidic sites ($mmolNH_3/g$) and surface area of metallic copper (m^2/g_{Cu}) after 20 h TOS (Fig. 22). The results showed a good correlation for structure insensitive characters of a direct synthesis of DME from syngas above the product value of 20 [138]. Since there is compensation effects of two variables between the metallic surface area of copper and acid sites on the zeolites during the precipitation-deposition method, TOF seems to be structure-insensitive reaction which indicates that the

Table 7
Pure and modified CZA/ferrierite catalysts.

Catalyst	Reaction conditions and catalytic activity							Ref.
	H_2:CO ratio	T (°C)	P (bar)	SV	X_{CO} (%)	Y_{DME} (%)	S_{DME} (%)	
CZA/FER	~1:1	250	40	5550 L/kgcat/h	30.2	–	28.7	[11a]
CZA/FER	2:1	270	30	8400/h	~14	–	~60	[118]
CZA/Zr-FER	~1:1	250	40	5500 mL/gcat/h	59.4	37.4	62.9	[94,137]
CZA/Zr-FER	~1:1	250	40	5550 mL/gcat/h	49.0	–	58.2	[133,136]
CZAZr/HFER	2:1	250	50	–	~38	–	~65	[135]
CZA/Al-FER	2:1	250	35	2000 mL/gcat/h	61.8	45.2	93.4	[138]

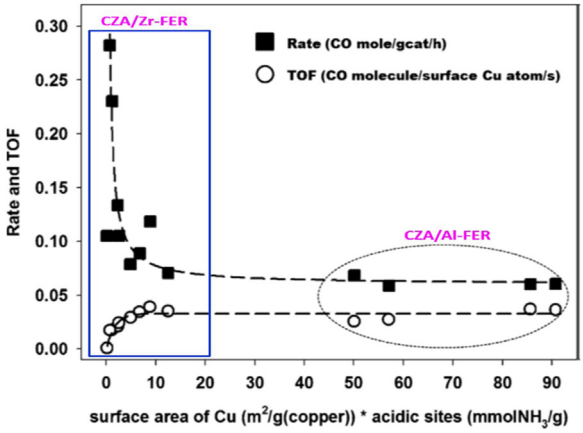

Fig. 22. Comparison study of reaction rate and intrinsic activity (TOF) of CZA/Zr-FER and CZA/Al-FER catalysts with respect to the product values of the amount of acidic sites ($mmolNH_3/g_{cat}$) and surface area of metallic copper (m^2/g_{Cu}) after reaction for 20 h [138].

higher metallic surface area on the solid-acid zeolites can suppress the acid site density on the zeolites through the selective deposition on the acid sites of zeolites.

3.3. Advanced methods for preparing hybrid catalysts

The common preparation methods for synthesis of hybrid catalysts for direct synthesis of DME are the coprecipitation of the MSC over the slurry of MDC or physical mixing of the individual components. However, some drawbacks in these methods are the randomly distributed active sites, and the inabilities to control the size of the precipitating particles and their subsequent aggregations. As a result, it is difficult for the hybridized catalysts to define separate reactions, methanol synthesis from syngas and methanol dehydration to DME, which can simultaneously happen on the active sites and suppress the side reactions as well [24]. Quite some emerging catalysts of finely designed structure have been proposed and well developed, among which the sonochemical-asssited, core-shell catalysts and physical sputtering are the most representative cases. As compared with the coprecipitation method alone, coprecipitation under influence of ultrasonic waves yields to fast nucleation rate, limited particle growth, strong interaction between particles and fragmentation of particle aggregates (Fig. 23) [139]. The nanocatalyst prepared by combined coprecipitation–ultrasound method revealed that the ultrasound energy enhanced dispersion of the CZA on the surface of HZSM-5 was coated uniformly (Fig. 23) and thus the highest activity of CO conversion (50.5%) with DME selectivity of 55%, as compared to coprecipitated–physical mixing method exhibited low CO conversion of 16.5% and selectivity of ~38% under the same reaction conditions studied [128]. To further enhance the STD perfomarance, the effect of each factors on sonochemical-asssited method was thoroughly studied and published from the same reseach groups [48,93,139–142].

Recently, Tsubaki group developed a millimeter-sized capsule catalysts by coating an acidic zeolite (shell) on a MSC pellet (core) for the direct synthesis of DME from syngas [143–145]. This novel tailor-made encapsulated method can weaken the interaction between MSC and zeolite and thus improve the reaction selectivity to DME. The formed methanol from the internal CZA core is given enough opportunities to contact the active sites of the HZSM-5 shell and is converted into the expected DME product (Fig. 24a), while complete absence of the unexpected hydrocarbon byproducts. The zeolite capsule catalysts with a synergetic confinement core shell structure at which the acidic zeolite shell enwrapped perfectly on the CZA core catalyst (Fig. 24b) [143].

Although the zeolite coated catalyst exhibited excellent DME selectivity, it hardly avoids the formation of the cracks and defects on the zeolite core structures during the acidic hydrothermal synthesis resulting in much lower CO conversion. The same authors also discussed the strategies for preparation of defect-free and compact HZSM-5 shell by dual-layer method where the formed silicalite-1 zeolite shell act as a protection layer, further facilitating the growth of the HZSM-5 shell under the stronger alkaline conditions [144,145]. For the STD conversion, the dual-layer capsule catalyst with Pd/SiO_2 core achieved a controlled reaction with excellent DME selectivity. Silicoaluminophosphate molecular sieves (SAPO) encapsulated methanol synthesis capsule catalyst were also prepared by simple physically coating method (Fig. 24c). This coating method is completely safe from cracks and defects caused by heat treatment and chemical corrosion. The researcher used SiO_2 as an adhesive for the preparation of a perfect shell of SAPO over Cr/ZnO [146] or CZA [147] as MSC core. In another study, Nie et al. [148] reported the special core–shell structured CuO–ZnO@HZSM-5 catalyst which was prepared by simple homogeneous precipitation through urea hydrolysis. The evolution of the capsule catalyst is further growing fast with few modifications for the STD reaction [149–153].

Although the varieties of catalysts and synthesis methods have been explored so far for DME synthesis, the catalytic activity of the hybrid catalysts decreases with time on stream owing to the deactivation by copper migration, oxidation, sintering [113,114,116,154,155], strong interaction between the CZA and the zeolite [114,116,117], coke deposition [105,108,111,154], and even contamination with impurities in syngas as well [46]. Therefore, several attempts have been made in the literature to improve the stability of Cu-based hybrid catalysts without affecting the catalyst activity of the STD process. In this sense, confining of copper nanoparticles within the zeolite matrix was proposed by Garciá-Trenco et al. [66] as an efficient strategy to improve the catalyst stability in the direct DME synthesis. Confinement on the Cu–ZnO catalyst inside the pores of the ordered mesoporous SBA-15 silica host prior to mixing with HZSM-5 is expected to avoid the direct contact of the active Cu sites with the zeolite surface and hence no detrimental interactions as well as to inhibit Cu sintering during the catalysis. HAADF-STEM image of Cu–ZnO catalyst (15Cu/Zn@S15)

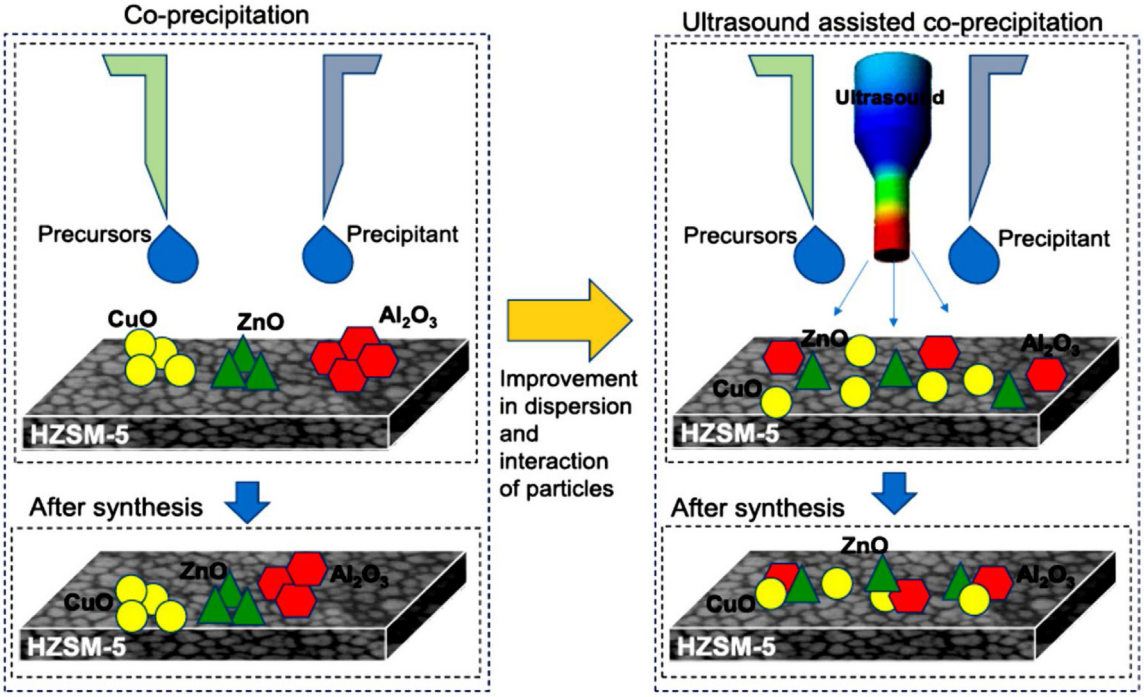

Fig. 23. Effect of ultrasound irradiation on the synthesis of the CZA/HZSM-5 nanocatalyst via the coprecipitation–ultrasound hybrid method [141].

showed that the SBA-15 channels were partially filled with Cu^0 nanoparticles (Fig. 25a), which having crystallite size of 5–6 nm and it was clearly evidenced by HRTEM (Fig. 25b). It was found that the confined copper catalyst deactivated at a much lower rate than the catalysts prepared by mixing or grinding method.

In another study, a series of highly dispersed Cu-Zn nanoalloys on HZSM-5 bifunctional catalysts were prepared via physical sputtering method by Tsubaki research group [119,156]. The sputtered catalyst was composed of well-dispersed Cu-ZnO nanoparticles of about 5 nm, which were physically anchored on the HZSM-5 support. However, the impregnated catalyst showed a wide particle distribution from 5 to 15 nm (Fig. 26). Interestingly an active Cu_5Zn_8 nanoalloy layer (Fig. 26a) was found after calcination and subsequent reduction of sputtered catalyst. The surface alloying and well-dispersed Cu-Zn nanoparticles played a cooperative catalytic role in improving STD performance, achieving a much higher DME selectivity of 92.1% and CO conversion of 13.7% than the conventional impregnated catalyst (selectivity of 76% and conversion of 3.5%). The "dry" sputtering route for catalyst preparation is a hopeful strategy to replace the conventional wet-chemical method, owing to its facile operation steps and being environmentally benign [24].

3.4. Reduction of the rate of WGS reaction

Most of the above works have been addressed either optimization of overall activity of the hybrid catalysts for the direct DME synthesis or lowering hydrocarbon production, though one cannot deny that the Cu-based MSC show activity for WGS reaction, which could result in the ample amount of CO_2 (Eq. (3)). It can be expected that an efficient promoter on hybrid catalysts would reduce the rate of WGS reaction. Few researchers were succeeded on reducing CO_2 selectivity by addition of some metal or metal oxides to the hybrid catalysts. For instance, Cai et al. [157] studied the electronic properties and surface distribution of Cu species were significantly changed by tin addition, suppressed the WGS reaction and therefore reduced CO_2 selectivity. Modification of HZSM-5 with the appropriate amount of MgO (<5 wt%) also decreased the amount of formation of both CO_2 and hydrocarbons with the parallel increase in DME selectivity (Table 8) [91]. Moreover, the proper acidity on zeolite can also suppress the formation of byproducts such as hydrocarbons and CO_2 [11,133]. A study reported by Li et al. [158] gave similar results after the addition of La_2O_3 promoter to Cu-ZrO_2/γ-Al_2O_3 with better catalytic performance as compared to Cu-ZrO_2/γ-Al_2O_3 hybrid catalyst.

4. Miscellaneous hybrid catalysts used for STD process

Research efforts have also been made on other hybridized bifunctional catalysts by choosing different combination of Cu-based MSC and MDC for the STD process. For example, a series of Cu–Mn–Zn/zeolite-Y prepared [73,110,159,160] and found an improved CO conversion and DME selectivity when the acidity of HY zeolite was modified via ion-exchange with rare earth [73] and transition [110] metals (Table 9). However, it is also important to mention that Cu–Mn spinel oxide with higher dispersion of metallic copper in the reduced catalyst could also showed a higher rate in WGS reaction [161]. Sun et al. [162] studied the effect of ZrO_2 as promoter on the CuO/ZnO/ZrO_2/HZSM-5 (CZZ/HZSM-5) instead of commonly used alumina and found increase in the activity and selectivity of the catalyst to DME by Cu^+ species stabilized by ZrO_2 in the presence of metallic Cu species.

Among different zeolites, as such or modified ZSM-5 and FER have been, so far, the most widely investigated for the STD process, though an alternative dehydration components such as H-mordenite (H-MOR) and H-MFI [50,51,71,163]; Al-modified MOR [164,165]; HMCM [112,120,166], metal-pillared ilerites [167,168] and natural clinoptilolite [169] with the Cu-based MSC have also been displayed good catalytic activity. SAPO was also used as methanol dehydration component in the hybrid catalyst [170,171]. The performance of the different bifunctional catalysts for the direct conversion of syngas to DME is summarized in Table 9.

From the reported results in Tables 2–9, some catalysts seem to outperform in terms of both the CO conversion and DME selectiv-

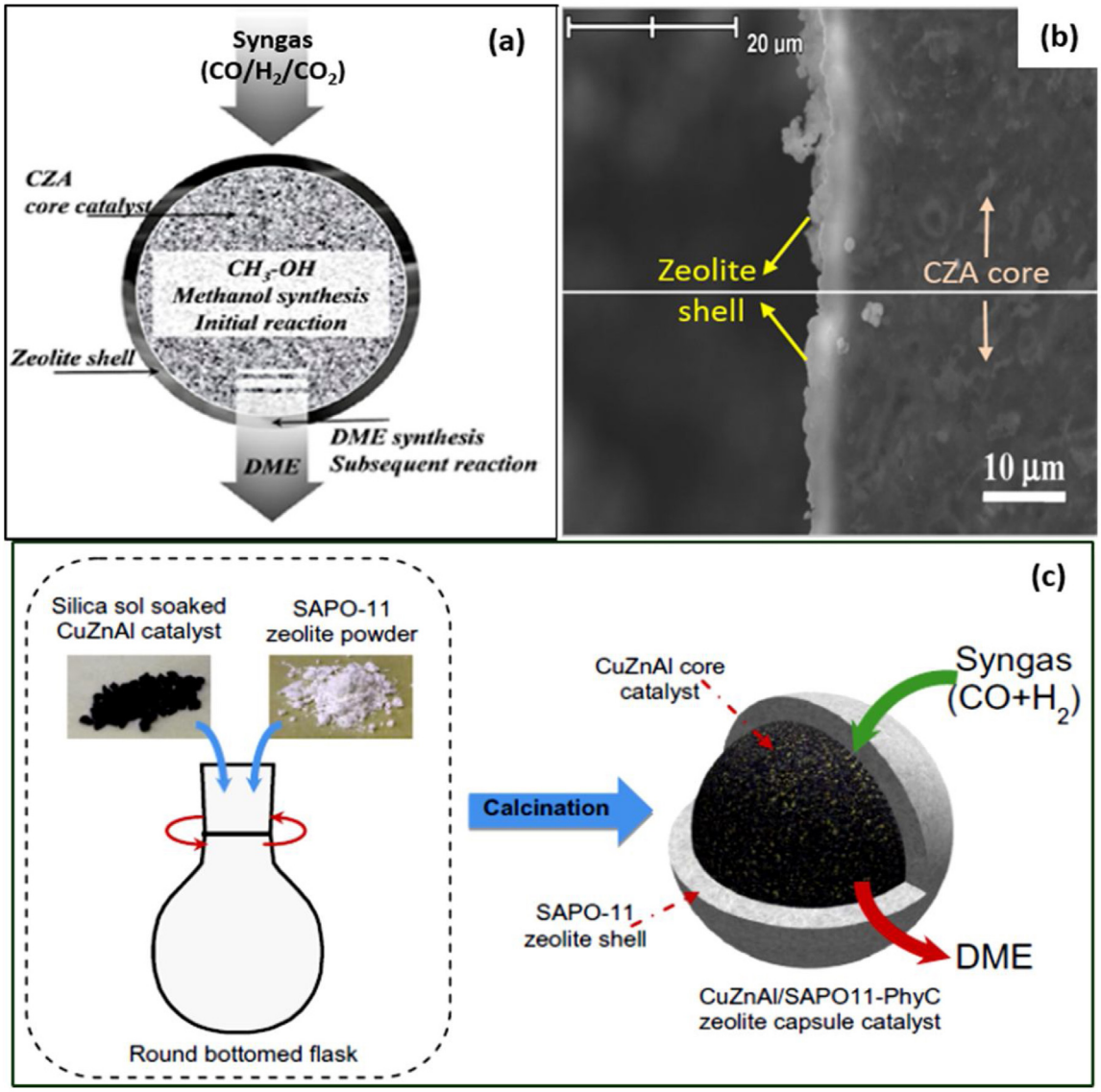

Fig. 24. (a) Reaction pathways and heat recycle on a single HZSM-5 capsule catalyst for DME synthesis; (b) Cross-section SEM image CZA@HZSM-5 capsule catalyst and (c) CZA/SAPO11 capsule catalyst prepared by physically coating (PhyC) method. [a,b taken from ref. [143] and c taken from Ref. [147]].

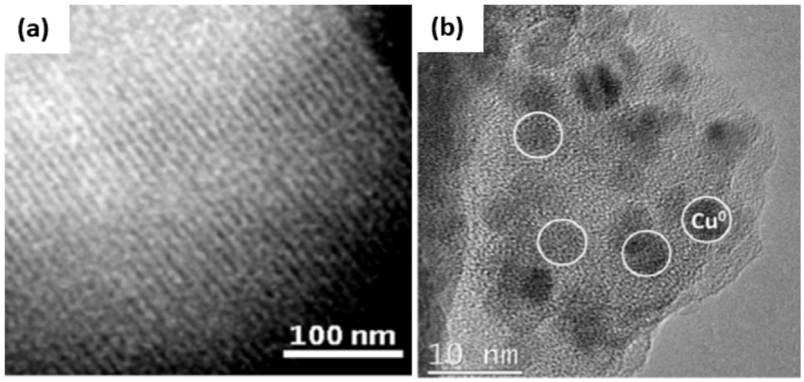

Fig. 25. (a) Representative HAADF-STEM and (b) HRTEM images of Cu–ZnO catalyst (15Cu/Zn@S15) [66].

ity. For instance, CO conversion of ~95% was reported over both CZA/alumina [55,78] and CZA/zeolites [91,120,132,134] catalysts under the reaction conditions employed. Similarly, the selectivity of DME was reported in the range of 93–97% [32,75,122,138]. However, it is worth to be noted that DME selectivities of >90% reported in the literature were mostly calculated on the basis of the organic products at which CO_2 was probably not considered as a product. So it is very difficult to compare these selectivities to that of obtained

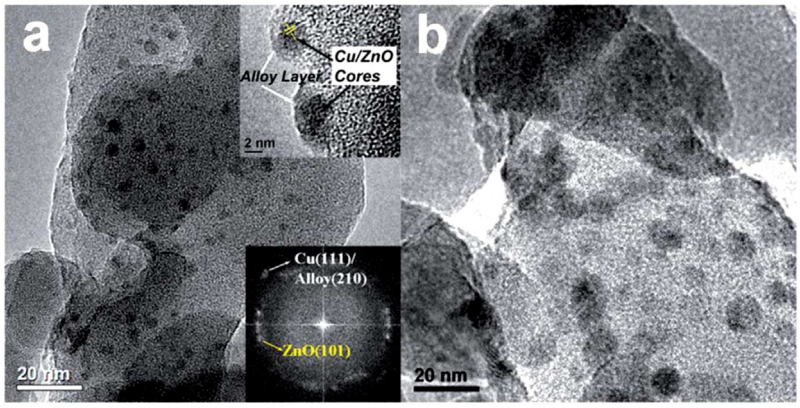

Fig. 26. HRTEM images of Cu-Zn/HZSM-5 (a) sputtered and (b) impregnated catalyst [119].

Table 8
Effect of modification of HZSM-5 with MgO on catalytic performance of CuO–ZnO–Al_2O_3/HZSM-5 for the direct synthesis of DME from syngas [91].

MgO content (wt%)	CO conversion (C-mol%)	Selectivity (C-mol%)			
		DME	Methanol	CO_2	Hydrocarbons
–	95.8	49.1	4.5	37.1	9.30
0.5	96.3	64.5	4.6	30.5	0.37
1.25	96.0	64.4	4.8	30.7	0.08
2.5	95.6	64.1	4.8	30.9	0.12
5.0	67.6	21.4	48.9	29.4	0.32
10.0	64.7	15.5	53.3	30.9	0.19

Table 9
Catalytic activity of other hybrid catalysts used for STD process.

Catalyst	Reaction conditions and catalytic activity							Ref.
	H_2:CO ratio	T (°C)	P (bar)	SV	X_{CO} (%)	Y_{DME} (%)	S_{DME} (%)	
Cu–Mn–Zn/Y	1.5:1	245	20	1500/h	53.6	–	63.5	[159]
Cu–Mn–Zn/HY	–	245	20	1500/h	66.6	–	67.0	[73]
Cu–Mn–Zn/La-Y	–	245	20	1500/h	76.7	–	66.6	[73]
Cu–Mn–Zn/Ce-Y	–	245	20	1500/h	77.1	–	66.7	[73]
Cu–Mn–Zn/Zr-Y	–	245	20	1500/h	71.4	–	67.5	[110]
Cu-Mn/Y	1.5:1	245	20	1500/h	25.4	–	62.6	[161]
CZZ/HZSM-5	2.2:1	250	30	1500/h	72.8	60.5	83.1	[162]
CZA/H-MOR	2:1	240	50	1100mLn/ g-cat/h	40.5	25.0	64.0	[50]
CZA/H-MFI90	2:1	240	35–50	1100mLn/ g-cat/h	80–84.0	47–55.5	61–66.7	[50,163]
CZA/H-MFI400	2:1	250	68	–	66.8	–	65.9	[51]
CZA/H-MOR90	2:1	250	68	–	37.0	–	25.2	[51]
CZA/H-MFI400	2:1	250	50	–	45.0	–	66.0	[71]
CZZ/Al-H-MOR	2:1	250	50	–	64–68.0	–	79–82.0	[164,165]
CZA/HMCM-22	2:1	260	40	1500/h	94–96.2	65.2	68.0	[112,120]
CZA/HMCM-49	2:1	260	40	1500/h	94.0	–	62.0	[166]
Cu/Zn-Ilerite	2:1	250	30	–	62–64.0	–	83–89.0	[167,168]
CZA/Clinoptilolite	2:1	275	40	–	26.0	–	45.8	[169]
CZA/SAPO-5	1.5:1	260	42	–	45.0	–	63.0	[170]
CZZ/SAPO-18	3:1	275	30	–	–	~16	~88	[171]
CZA/FER[a]	2:1	250	50	2000 mL/gcat h	91.3	57.7	63.2	–

[a] Our recent results on the physically mixed CZA/FER(PM, highly crystalline)) with the weight ratio of CZA/FER = 5.

from other methods. On the other hand, a lower activity in the WGS reaction was reported as the reasons for the exceptionally higher DME selectivity as well [76,119,129]. By comparing selectivities of DME only without mentioning the CO conversion, or vice versa, over different catalytic systems may be meaningless. Therefore, a proper comparison of the catalytic activity of the different catalytic systems can be viable when the reactions have been performed under comparable reaction conditions such as temperature, pressure, H_2/CO ratio, catalyst amount, space velocity and composition of feed gases besides the catalyst properties.

5. DME production from CO_2/H_2 mixtures over hybrid/bifunctional catalysts

Syngas-based production of methanol and subsequently DME formation inevitably generates certain amounts of CO_2 according to the Eq. (4) [172]. Furthermore, DME and all carbon-containing fuels upon their combustion generally form the chemically stable CO_2 product. Chemical recycling of CO_2 to the renewable fuels and value-added chemicals offers an influential alternative to tackle both global climate change and fossil fuel depletion. However, the use of CO_2 as chemical feedstock is limited due to its highest thermodynamic stability and thus high energy substances or elec-

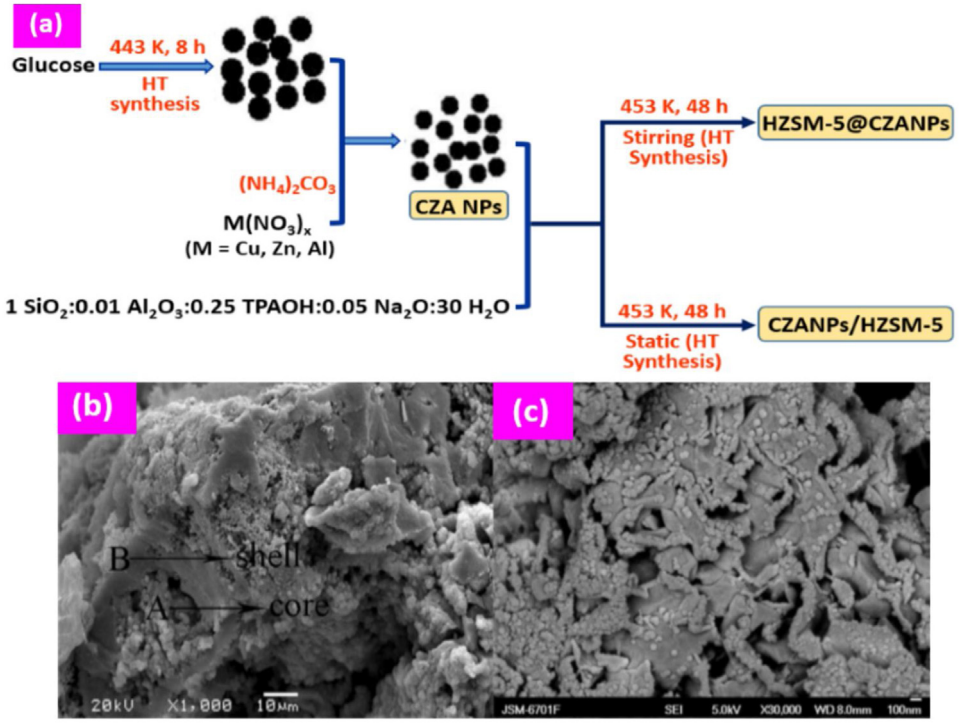

Fig. 27. (a) Preparation procedure of HZSM-5@CZANPs (core-shell-like structure) and CZANPs/HZSM-5 hybrid catalysts with their SEM image in (b) and (c), respectively [187].

troreductive processes are typically required to transform CO_2 into other chemicals [173]. Hydrogen, a high energy material obtained either from fossil resources or through water splitting, can be used as a proper reagent for CO_2 activation and transformation [174]. Therefore, the hydrogenation of CO_2 reaction offers the challenging opportunities for sustainable development in energy and the environment. The CO_2 utilization approach to fuels like DME synthesis is still an early stage for scientists, even though it is relatively mature to chemical synthesis like urea and carbonates. However the worldwide requirements of fuels are nearly two orders of magnitude larger than that of the chemical intermediates [175].

A number of investigations such as the effects of active components [176], supports [177], promoters [176a,178], preparation methods [179] and calcination temperature [179a] have been extensively studied for direct synthesis of DME from CO_2. However, in spite of these efforts, the studies on CO_2 hydrogenation to DME synthesis are few with low yield of DME as compared to hydrogenation of CO to DME [180]. Also in contrast to CO hydrogenation, more water is produced in CO_2 hydrogenation via reverse water gas shift (RWGS) reaction (Eq. (7)) which decreases the methanol synthesis reaction rate [174]. Indeed, the conventional Cu/ZnO-based MSC catalysts which are not only active for methanol synthesis, but also active for both WGS (Eq. (3)) as well as RWGS reactions (Eq. (7)) [179c,181].

$$CO_2 + H_2 \leftrightarrow CO + H_2O \quad \Delta H^o = -41.2\,kJ/mol(RWGS) \qquad (7)$$

Thermodynamically, a decrease of the reaction temperatures or an increase of the reaction pressures can favor the direct synthesis of DME from hydrogenation of CO_2 [32,182]. Chen et al. [32] have conducted a kinetic and thermodynamic study by varying the reaction temperature. At lower temperatures (<225 °C), the reaction is dominated by chemical kinetics, whereas for higher temperatures (>225 °C), the thermodynamic equilibrium dominates the reaction. Moreover under kinetic conditions, the CO concentration dramatically increases with increasing temperatures, hence low reaction temperature could be an answer to improve the methanol/DME productivity from hydrogenation of CO_2 [30a,183]. Su et al. [184] described that the activation of CO_2 under the plasma condition can reduce the activation energy of the CO_2 hydrogenation reaction resulted in improving the yield of DME by maintaining the synergistic effect between the plasma and the active sites on the hybridized bifunctional catalysts.

Many researchers demonstrated that the combination of Cu-based MSC with the solid acid catalysts certainly provide a strong driving force for CO_2 conversion. Although Cu remains the main active catalyst component, the different modifiers such as Cr, Zn, Al, Zr, Fe, Ce, Ti, V, La, Mo, Pd, Nb and Ga have been tested for methanol synthesis from hydrogenation of CO_2 [178–180,185–204]. An appropriate modifier not only affects the interactions between the major component and promoter but also is capable of tuning active sites of the catalysts. In general, the CZA/zeolites hybrid catalysts for CO_2 hydrogenation show the better performances in terms of the activity and hydrothermal stability than that of the CZA/γ-Al_2O_3 catalysts [129,181,186,205]. For instance, CZA/HZSM-5 catalyst favored a stable activity with higher CO_2 conversion of 20%, 29% and selectivity to DME 53%, 65% in the slurry and fixed-bed reactors, respectively. Nevertheless, the catalyst CZA/γ-Al_2O_3 was found to be unstable in the slurry reactor showed low conversion (10%) and selectivity to DME (4%) because CO produced as the main product (58%) by the RWGS reaction [181]. Furthermore, the simulation study predicted that the zeolite membranes with MSC always promote a high CO_2 conversion into DME [186,205].

Table 10 shows the catalytic materials that have been used for direct DME synthesis by CO_2 hydrogenation. The hybrid catalysts having important factors such as dispersion, crystallite size and surface area of metallic Cu, and nature of acid strength along with acid sites of zeolites played a vital role for direct DME synthesis from hydrogenation of CO_2. These features have already been explained well in previous part of this review (Section 3.2). Nevertheless, in the context of the present section of CO_2 hydrogenation to DME few salient features are mentioned briefly to understand the physicochemical–activity relationships.

Table 10
Direct DME synthesis by hydrogenation of CO_2 over hybrid/bifunctional catalysts.

Catalyst	Reaction conditions and catalytic activity							Ref.
	H_2:CO_2 ratio	T (°C)	P (bar)	GHSV	X_{CO2} (%)	Y_{DME} (%)	S_{DME} (%)	
Cu-ZnO/Al_2O_3	3:1	270	30	–	7.0	–	35.0	[185]
CZA/γ-Al_2O_3	4:1	275	40	–	~17.0	~9.0	–	[183b]
CZA/NaHZSM-5	2:1	275	40	–	35.0	25	77.5	[129]
CZA/NaHZSM-5	4:1	275	40	–	–	~20	~50	[186]
HZSM-5@CZA	3:1	270	30	1800 ml $gcat^{-1}$ h^{-1}	48.3	23.4	48.5	[187]
CZA/ZSM-5	3:1	260	50	3000 mLg^{-1}	29.0	–	65.0	[181]
CZA/HZSM-5	10:1	280	360	10,471/h,	97.0	–	89.0	[188]
CZA/HZSM-5	3:1	270	30	4200/h	30.6	15.1	49.2	[189]
CZAZ/HZSM-5	3:1	260	30	1600/h	25.2	5.8	23.2	[190]
CNTs-CZA/HZSM-5		260	30	1800 mLg^{-1} cat/h	46.2	20.9	45.2	[177a]
La-CZA/HZSM-5	3:1	250	30	3000/h	43.8	–	71.2	[191]
CZA/MOR	3:1	240	30	620/h	25.0	–	55.1	[192]
CZA/silica-alumina	3:1	250	30	–	20.0	7.2	–	[193]
CZA@amorphous silica-alumina	3:1	266	30	1800 mL $g_{cat}{}^{-1}$ h^{-1}	47.1	19.9	42.4	[194]
ZCZ/HZSM-5	3:1	220	30	4500 NL/kgcat/h	13.6	–	42.0	[195]
CZZ/HZSM-5	3:1	250	30	3600 mL g^{-1} h^{-1}	22.2	15.0	67.6	[179a]
CZZ/HZSM-5	3:1	220	9	–	~7.5	–	~40	[179b]
V-modified CZZ/HZSM-5	3:1	270	30	4200/h	32.5	19.1	58.8	[196]
CuZr–PdCNTs/HZSM-5	3:1	250	50	25,000 mL/(h g-hydr. catal)	18.9	–	51.8	[197]
CZZ/MFI	3:1	240	50	2500 NL/kgcat/h	23.6	11.6	49.3	[198]
CZZ/FER	3:1	260	50	8800 NL/Kgcat/h	23.6	–	47.0	[179c]
CZZ/SZ	3:1	260	20	–	4.0	3.5	–	[199]
CZZ/H-Ga-silicate	3:1	250	28	–	19.0	–	45.3	[180]
0.5 Pd-Cu–Zn–Al–Zr/HZSM-5	3.3:1	200	30	1800/h	18.7	–	73.6	[179d]
CuO–TiO_2–ZrO_2/HZSM-5	2.8:1	250	30	1500/h	15.6	7.4	47.5	[200]
CuO–Fe_2O_3–ZrO_2/HZSM-5	5:1	260	30	1500 mL $g_{cat}{}^{-1}$ h^{-1}	28.4	–	64.5	[201]
Cu-Fe-Ce/HZSM-5	4:1	260	30	1500 mL $gcat^{-1}h^{-1}$	18.1	9.4	52.0	[202]
Cu-Fe-Ce/HZSM-5	4:1	260	30	1500 $mgcat^{-1}$ h^{-1}	20.9	13.2	63.1	[177b]
Cu-Fe-Ce/HZSM-5 + plasma	4:1	260	30	2000 mL $gcat^{-1}h^{-1}$	24.3	16.9	69.5	[184]
Cu/ZnO/Ga_2O_3/H-Ga-silicate	3:1	250	28	–	19.4	–	19.9	[180]
Pd–Nb_2O_5/LS-Ga_2O_3	7.5:1	270	17	–	5.0	–	53.0	[203]
Cu–Mo/HZSM-5	3:1	240	20	1500/h	12.4	–	77.2	[31]
CuCe/V-Al PILC	3:1	250	40	20.000 L $kgcat^{-1}h^{-1}$	~5	–	~50	[204]
CZA/FER(PM)[a]	3:1	250	50	2000 L $kgcat^{-1}h^{-1}$	38.7	31.0	80.1	–

[a] Our recent results on the physically mixed CZA/FER(PM, highly crystalline) with the weight ratio of CZA/FER = 5.

Erena et al. [129] studied the initial evolution of CO_2 conversion and DME yield with time on stream at different H_2/CO_2 molar ratios (1:1 to 8:1) in the feed over CZA/NaHZSM-5 hybrid catalyst. They obtained 35% CO_2 conversion with DME yield of ~25% in 2 h at 275 °C with H_2/CO_2 molar ratio of 3:1. In order to confirm internal diffusion (catalyst pores), and external diffusion (stationary outside particle layer), the reaction was carried out varying the particle size (0.2, 0.45 and 0.9 mm) and observed that the reaction is not affected by any diffusional restrictions. Zhang et al. [189] prepared the CZA by simple urea–nitrate combustion method and then physically mixed it with HZSM-5. The results show that the amount of fuel (urea) has a great influence on the physiochemical properties of the catalysts. Arena et al. [179a] also found that the combustion route ensures the best cooperation in terms of Cu dispersion, which results in higher methanol productivity rate. Bansode et.al, proposed a very high-pressure approach (360 bar) using CZA/HZSM-5 bifunctional catalyst for direct synthesis of DME from CO_2 hydrogenation remarkably boosted DME selectivity of 89% with CO_2 conversion of 97% [188].

Liu et al. [187] prepared CZA composite nanoparticles (CZANPs) using carbon sphere as template which obtained from glucose source. The HZSM-5@CZANPs (core-shell-like structure) and CZANPs/HZSM-5 hybrid catalysts were prepared hydrothermally (HT) by adding CZANPs and HZSM-5 membrane in continuous stirring and static conditions, respectively (Fig. 27a). From the SEM image of HZSM-5@CZANPs (Fig. 27b), it can be clearly observed the core–shell-like structure in which CZANPs distributed quite homogeneously on the surface of the HZSM-5 and the thickness of the defective layer was found to have 3–5 μm. However, the catalyst obtained by static conditions didn't show any core-shell-like structure (Fig. 27c). Though both HZSM-5@CZANPs and CZANPs/HZSM-5 were displayed almost comparable CO_2 conversion (45–48%), the former catalyst possesses a higher yield of DME (23.4%) than that of CZANPs/HZSM-5 (17%) under the reaction conditions studied.

In another interesting work reported by Zha et al. [194], a core-shell-like structure of CZA metal oxide cores enwrapped by one layer of a metal-doped amorphous silica-alumina (ASA) membrane. The capsule catalyst with CZA cores was prepared by co-precipitation using urea with *n*-butylamine (CZAZb), and it exhibited high conversion of CO_2 (47.1%) and 19.9% yield of DME compared with the conventional CZA hybrid catalyst (CZAaZ) which showed ~30% CO_2 conversion with 10% DME yield. The improvement in the catalytic activity of the CZAZb was correlated with an increase in acidity brought about by the enhanced condensation of the alumina-silicate frameworks in the ASA structures, which was generated by better incorporation of Al species due to Al migration from the CZA core region. This hypothesis was confirmed by analyzing powder X-ray diffraction (PXRD) pattern of the CZAZ catalysts. The PXRD pattern of the residual solid, which was collected by centrifugation after the hydrothermal synthesis to know the unwrapped amorphous silica-alumina (RASA), CZA, CZAZ (capsule catalyst) and CZAM (prepared by mechanical mixing CZA with ASA) are shown in Fig. 28. There were distinctive changes in the PXRD pattern of RASA showing the CuO, Cu_2O, and ZnO peaks, which indicated that some Cu^{2+} and Zn^{2+} migrated from the core to the precursor solutions. On the other hand, the relative intensities of the CuO, ZnO, and Al_2O_3 peaks increased in the PXRD pattern of CZAZ and CZAM due to the metal oxide cores, as the intensity of the amorphous peaks was weak compared with the same peaks in pure RASA.

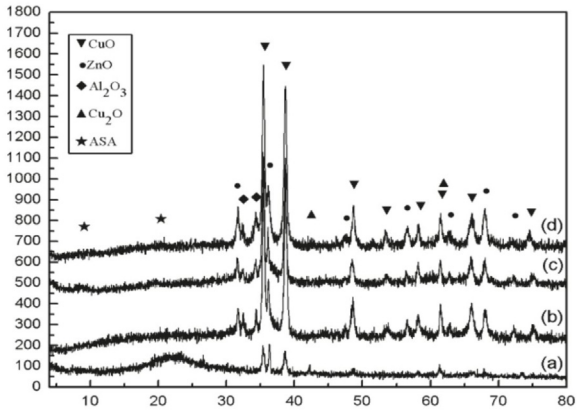

Fig. 28. PXRD pattern of (a) RASA (centrifuged residual liquid of amorphous silica-alumina, (b) CuO-ZnO-Al_2O_3, (c) CZAZ (amorphous silica-alumina capsule catalysts), (d) CZAM (mechanically mixed CZA with amorphous silica-alumina) [194].

It is also noteworthy that copper particles promoted on the ZnO/ZrO_2 (CZZ) have attracted much attention due to its high stability in water and less deactivation, compared to the conventional CZA catalyst, for the synthesis of methanol from CO_2 hydrogenation [206]. It seems that the Zr incorporation to the MSC can change the outer-shell electrons of Cu species, improve the reducing behavior of CuO, and increase the surface area and the number of active sites, thus clearly promotes the conversion of CO_2 and the yield of DME [24]. On the other hand, a strong hydrophilic character of alumina carrier promotes the poisoning effect of water on active sites and thus depresses the CO_2 hydrogenation functionality over conventional CZA-based catalysts [207]. According to Frusteri et al. [208], on the CZZ/HZSM-5 hybrid system, H_2 is initially adsorbed and activated on the Cu^0 sites, while CO_2 is adsorbed on the basic surface sites of ZnO and ZrO_2 forming activated CO_2. Subsequently, the activated H_2 spill-over to the activated CO_2 leads to formation of intermediates namely formate that stabilized at the metal-oxide interface prior to formation of methanol from the hydrogenation reaction [209]. Density functional theory analysis also revealed the formate pathway for methanol synthesis from CO_2 hydrogenation preferentially [210]. Fig. 29 shows the species that more likely present on the surface of the CZZ methanol catalyst and the distinct role of Cu, Zn and Zr centers [207].

Bonura et al. [183a,195] prepared Cu–ZnO–ZrO_2 (ZCZ) by a reverse co-precipitation method under ultrasound irradiation and then four different combination procedures (Fig. 30a) were adopted to get a hybridized bifunctional catalysts (ZZ) with HZSM-5. TEM image of ZZ-G (grinding method) displayed the isolated metallic copper particles which were distributed over HZSM-5 matrix randomly (Fig. 30b) due to mechanical stress induced during grinding of each components. On the contrary, the co-precipitated ZZ-C catalyst shows dispersed metal-oxide(s) particles on HZSM-5, with a rather uniform size distribution. ZZ-M, a combination of the two physically mixed components, merely features the isolated structure of methanol ZCZ catalyst and HZSM-5 without any evidence of intimate chemical interaction (Fig. 30b). Although the rate of DME production on ZCZ and ZZ-C is close to zero, 20% CO_2 conversion rate enhanced was observed over ZZ-C hybrid catalyst as compared to ZCZ alone (Fig. 30c). Very small amount of DME formation on ZZ-C may be due to the disappearance of weak to medium acid sites of HZSM-5 is expected during the co-precipitation step, causes an ionic exchange of acid sites of zeolite with metal precursors of ZCZ catalyst. On the other hand, ZZ-G catalyst exhibits a lower CO_2 conversion with appreciable DME production rate (3.2 mmol $kg_{ZCZ}^{-1}s^{-1}$), though mechanical stress induced by grinding that caused a detrimental interaction among the active sites. Two sequential catalytic beds within the same reactor (ZZ-D), in which methanol formed in the first step on ZCZ is converted into DME on acid sites of HZSM-5 in the second step, attains an enhancement of both CO_2 conversion and DME production rate with respect to the reference system (*i.e.* ZCZ). Among all catalysts studied, the NH_3-TPD profile of ZZ-M catalyst exhibited three well resolved peaks centered at 505, 684 and 824 K (Fig. 30d), as a result of the contribution of the acid sites of zeolite (low and medium temperature) and ZCZ (high temperature) and thus the highest rate, both in terms of CO_2 conversion (8.4 mmol $kg_{ZCZ}^{-1}s^{-1}$) and DME production (4.4 mmol $kg_{ZCZ}^{-1}s^{-1}$) (Fig. 30c).

The same research group also studied the influence of catalyst preparation method and zeolite topology, in order to optimize the system in terms of physico-chemical properties and catalytic activity [179c,198,208,211]. They found that the methanol synthesis catalyst obtained from gel-oxalate coprecipitation method with 2-D zeolite framework of FER demonstrated higher DME yield than obtained using other methods and zeolites. The image mapping from EDAX measurements of the catalyst surfaces evidenced the gel-oxalate coprecipitated catalyst (OX-FER/2) displayed uniform mixing of each active sites favors the mass-transfer during the STD reaction, while the existence of lack of homogeneity in the element distribution of the impregnated catalyst (IW-FER/2) (Fig. 31). Nevertheless, the EDAX results of catalysts prepared by gel-oxalate coprecipitation and wet impregnation method show a similar average composition (Fig. 31) [179b]. Compared with these coprecipitation and impregnation methods, the solvent-free method of solid-state reaction between hydrated metal salts with oxalic acid was found to be a simple as well as efficient method for the preparation of CZZ/HZSM-5 bifunctional hybrid catalyst [179a].

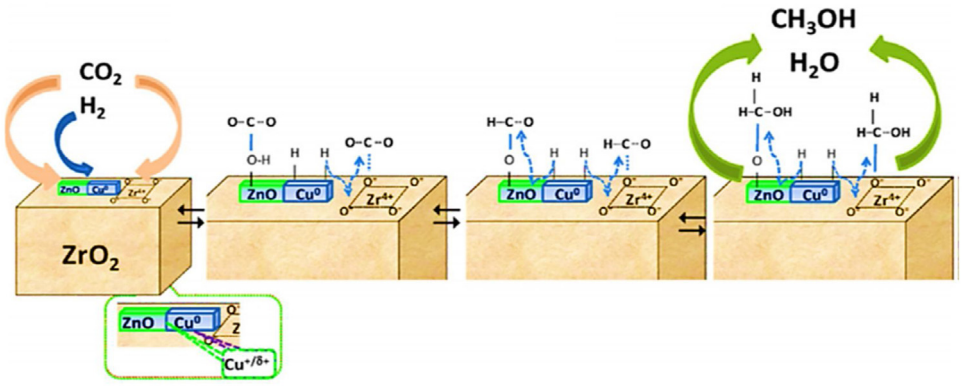

Fig. 29. CZZ catalysts surface and functionality of the various surface sites for methanol synthesis via CO_2 hydrogenation reaction [207].

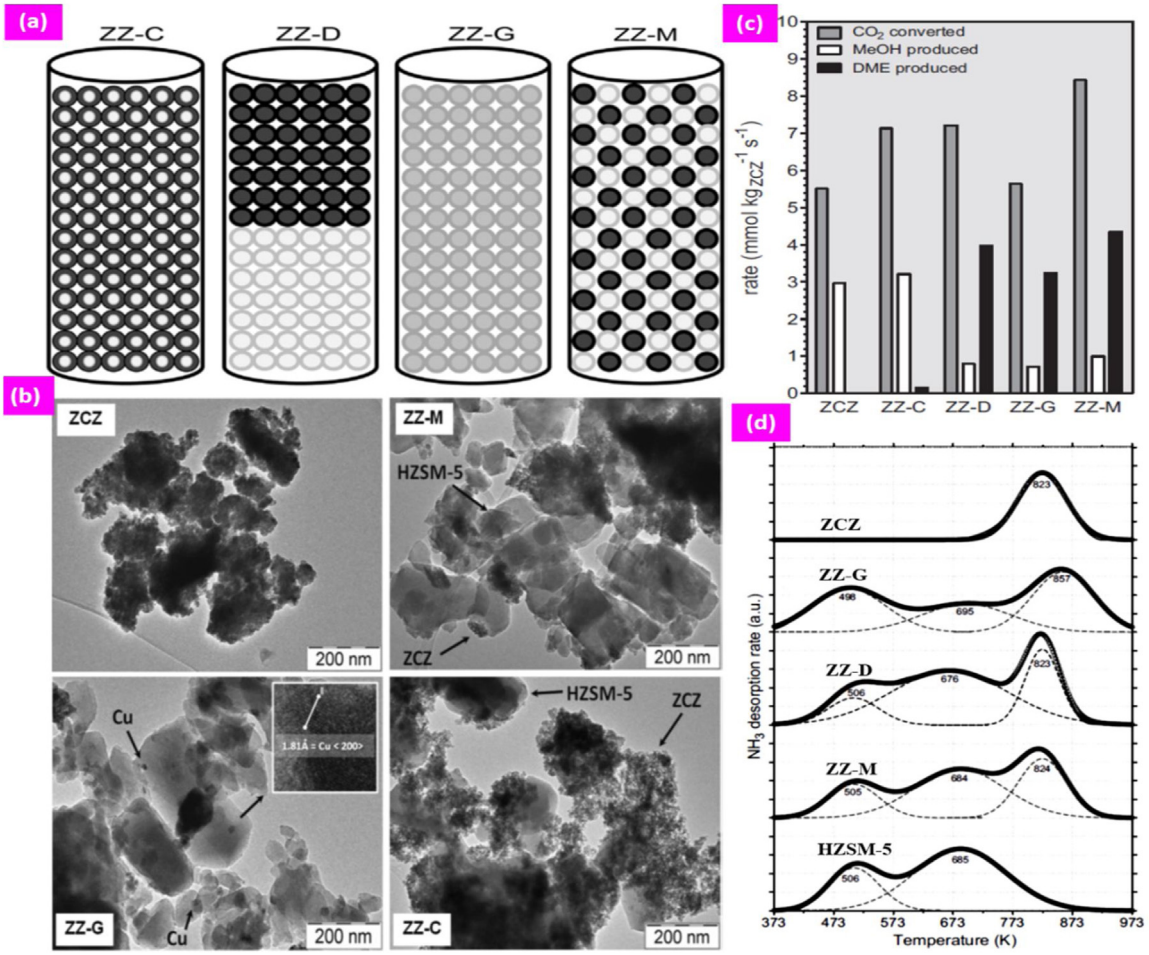

Fig. 30. (a) Combination procedures between methanol synthesis (● = ZCZ) and methanol dehydration (○ = HZSM-5) catalysts. (ZZ-C obtained from ZCZ metallic precursor solution mixed with finely dispersed HZSM-5 under ultrasound irradiation; ZZ-D derived from dual-bed of same-size ZCZ (first bed) with HZSM-5 in second bed; homogeneous solid mixture of each components prepared by grinding (ZZ-G) and physical mixture of same-sized components gave ZZ-M bifunctional catalyst); (b) TEM images, (c) the reaction rate for the hydrogenation of CO_2 and (d) NH_3-TPD deconvolution profiles of catalysts prepared by different methods [a,b and c taken from Ref. [195] and d taken from Ref. [183a]].

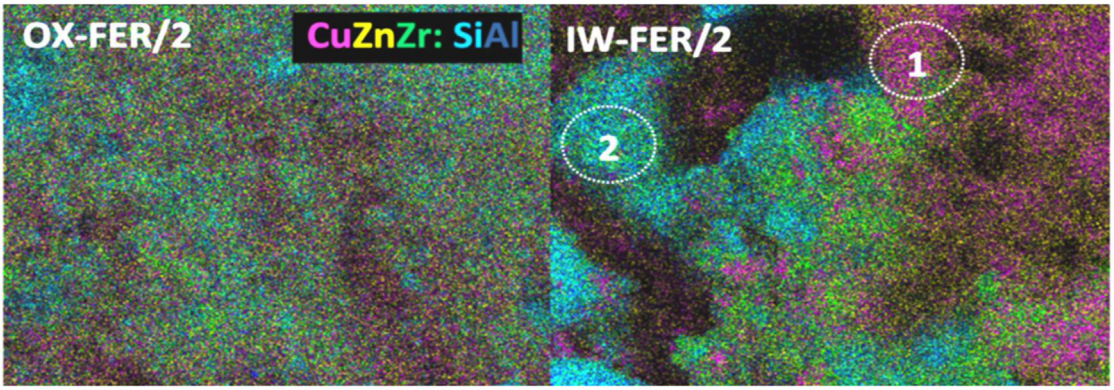

	Composition (wt. %)				
	CuO	ZnO	ZrO_2	SiO_2	Al_2O_3
OX-FER/2	34.87	18.85	10.94	31.74	3.60
IW-FER/2	34.48	16.71	14.42	30.30	4.09
Zone 1	70.40	16.58	8.88	3.45	0.69
Zone 2	14.74	9.58	12.23	55.89	7.57

Fig. 31. Mapping investigations with results of EDAX measurements on the reduced OX-FER/2 and IW-FER/2 samples [179c].

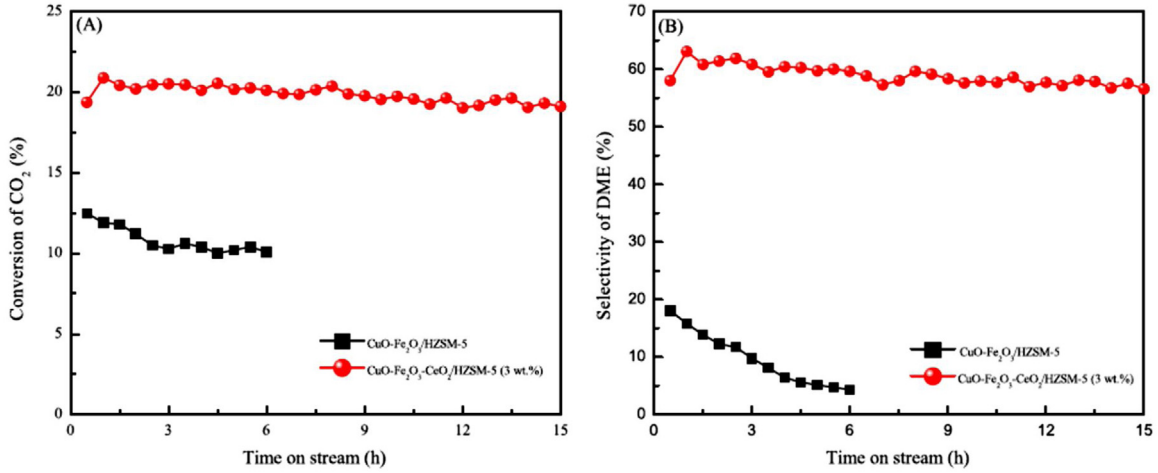

Fig. 32. Effects of (A) the conversion of CO_2 and (B) the selectivity of DME with and without CeO_2 on CuO–Fe_2O_3/HZSM-5 based on time on stream stability [177b].

Park et al. [180] compared the catalytic activity of hybrid catalyst of CZZ and Cu/ZnO/Ga_2O_3 with H-form Ga-silicate for CO_2 hydrogenation. They found that the hybrid catalysts composed of the CZZ showed a higher selectivity to DME (45.3%) than that of the Cu/ZnO/Ga_2O_3 (19.9%), although the conversion of CO_2 was found to be comparable (~19%). On the contrary, Jun et al. [176a] have screened various metal oxides including Al_2O_3, Cr_2O_3, Ga_2O_3 and ZrO_2 to enhance Cu/ZnO dispersion, and found that the most promising catalyst was Cu-ZnO-Cr_2O_3 with CuNaY as the dehydration catalyst. The addition of Cr_2O_3 increases the DME selectivity significantly than that of the Al_2O_3 and ZrO_2.

Wengui et al. [191] modified the conventional CZA catalyst by adding different amount of La (1–8 wt%) and found that optimal La enhanced the dispersion of copper particles and reduce the CuO crystallite size. Addition of an appropriate amount of zirconia promoted the activity of CZA catalysts for DME synthesis [190,205a]. It is believed that the added zirconia not only reduce Cu/Zn sintering but also offers a positive ion defects on the surface of Cu-ZnO. Furthermore, the addition of Pd to Cu–Zn–Al–Zr/HZSM-5 clearly enhanced the DME selectivity and retards CO formation, probably due to the spillover of hydrogen from Pd^0 to the neighboring phase [179d]. Zhang et al. [196] reported that by adding 0.5 wt% V_2O_5 onto a CZZ/HZSM-5 (CZZ$V_{0.5}$H), CO_2 conversion and DME selectivity increased to 32.5% and 58.8% compared to those for the unmodified CZZV_0H catalyst exhibited 28.9% CO_2 conversion with 55.1% DME selectivity.

Recently, carbon nanotubes (CNTs), act as a novel supporting materials or promoters, have drawn increasing attention for the direct synthesis of DME [89,177a,197]. The Pd-decorated CNTs promoted Cu-ZrO_2/HZSM-5 (CuZr–PdCNTs/HZSM-5), showed an excellent capability to adsorb the reactants of H_2 and CO_2, and played an important role in facilitating the increase of specific reaction rate of CO_2 hydrogenation [197]. Besides, addition of metal oxide promoters such as Ti [200], Fe [201,210], Ga [176a,180] and Cr [176a] to Cu-ZrO_2, and Mo [31], Ce and Nb [204] to Cu particles leads to an increase in yield of DME. For example, Qi et al. [31] found that a small amount of MoO_3 addition not only produces new adsorption sites but also enhances binding of adsorbate on the catalyst surface. Apart from these catalysts, the CeO_2 modified CuO-Fe_2O_3 catalysts formed a stable solid solution, which decreased the reduction temperature of highly dispersed CuO and altered the specific surface areas, and thus improved the catalytic activity [177b,202]. Moreover, the adsorbing capacity of H_2 and CO_2 increased after Zr-doping to Cu–Fe methanol catalyst [210]. During 15 h time on stream, CO_2 conversion and selectivity of DME remained nearly constant, compared to the catalyst without addition of CeO_2 promoter, as shown in Fig. 32 [177b].

It is important to remind that the strong acid sites of zeolite is also active for the transformation of DME into hydrocarbons, which partially develop to coke that could block pores of zeolite causing deactivation [174]. Therefore, the selection of dehydration catalysts is particularly noteworthy. Jun et al. [176a] claimed that CuNaY is an excellent dehydration catalyst attributed to the presence of a moderate acid strength. Pillared clays have been studied as methanol dehydration catalyst due to their low cost. The addition of aluminum in the pillared clays (V-Al PILC) leads to significant modifications in their acidity, which is due to the increase of specific surface area and formation of new acid sites [204]. The modified zirconia with sulfate species was reported to increase the dehydration rate and minimize the coke formation [199]. However the physicochemical properties, activity and stability of the sulfated zirconia catalysts (S-ZrO_2) were strongly affected by sulfur content on the zirconia surfaces. The sulfur content and the nature of sulfate binding with zirconium atom strongly influence the strength and type of acidity in the catalyst [212]. For example, at low sulfur loading of 5 (5S-ZrO_2) and 10 wt% (10S-ZrO_2), the tridentate sulfate was favorably formed on the zirconia surfaces and induced zirconium atoms to act as the weak Lewis acid sites. However at high sulfur contents (15S-ZrO_2, 20S-ZrO_2 and 30S-ZrO_2), a protonated sulfate species was formed and donated significant Brønsted acidity, which efficiently catalyzed the methanol dehydration even at a relatively low reaction temperature (260 °C). The S-ZrO_2 catalyst with 20 wt% sulfur loading achieved a superior DME productivity of 236 gDME kg_{cat}^{-1} h^{-1} at 260 °C in 20 bar [199]. An increase in DME yield was observed in all the reaction temperatures with increasing the total number of acid sites (Fig. 33a). The mechanism of methanol to DME reaction also depends upon the amount of sulfur content present on the S-ZrO_2, as shown in Fig. 33b and c.

On both CO or CO_2 hydrogenation, the surface acidity from solid acid catalysts and metallic sites for hydrogenation are crucial factors to explain the catalytic performances and the selection of the proper hybridized bifunctional systems with catalyst preparation methods can also inevitably important for the STD reaction.

6. Conclusions and outlook

DME, the smallest aliphatic ether with no C—C bond structure, can be used as an excellent alternative to diesel fuel, LPG and methanol fuels. DME can be synthesized either by a single-step (direct synthesis) or the two-step (indirect synthesis) methods

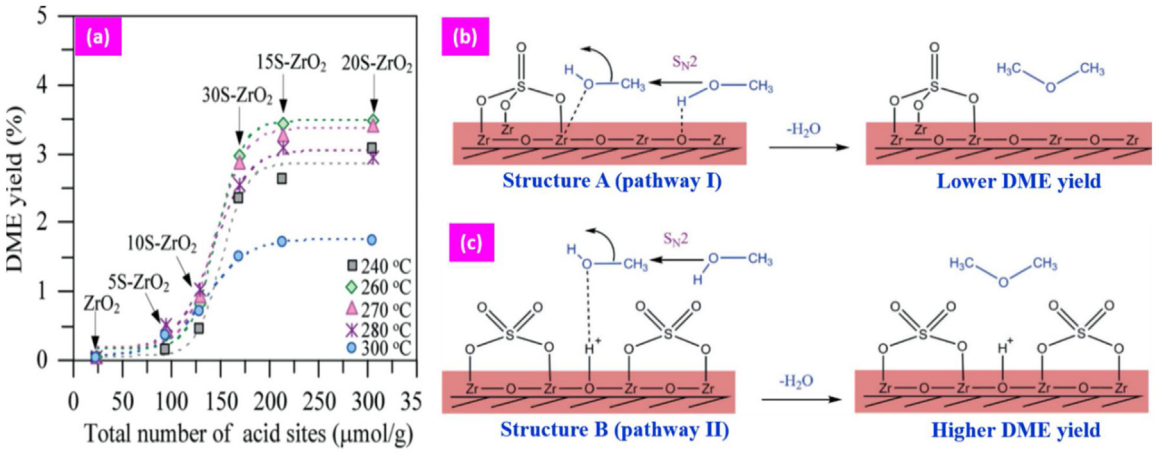

Fig. 33. (a) Correlation of DME yield with the total number of acid sites at different reaction temperatures, proposed mechanism for the formation of DME from methanol dehydration over the sulfated zirconia catalysts at (b) low (structure A) and (c) high (structure B) sulfur contents [199].

from syngas. In the indirect synthesis method, methanol is synthesized from syngas on a metallic copper-based catalyst in the first step, limited by the thermodynamics, followed by methanol dehydration by solid acidic catalysts such as γ-alumina and zeolites mainly. On the other hand, the direct DME synthesis, which simultaneously triggering methanol synthesis and *in-situ* dehydration can be integrated in hybridized bifunctional catalysts in a single reactor, alleviates the thermodynamic constraints of methanol synthesis. From both the cost and product-yield points of view, the direct synthesis of DME from syngas may be the preferred route for large scale industrial production. Furthermore syngas-to-DME (STD) is one of the hot research areas in energy chemistry and sustainability standpoint as syngas is produced from any carbon resources like natural (or shale) gas, coal and biomass. Also DME can be processed into valuable co-products such as hydrogen as a sustainable future energy.

The conversion of STD can be conducted over dual catalytic systems, which were varied from a physical mixture of Cu-based methanol synthesis component with solid acid one to hybridized bifunctional catalysts via the coprecipitation or mixing of the freshly precipitated precursors. Compared to the conventional physical mixing or coprecipitation methods, the sonochemical-asssited and physical sputtering methods were reported to have finely designed structure that exhibit strong interaction between particles and a homogeneous distribution of methanol active sites on supports. Oxidation state, dispersion and crystallite size of the metallic Cu particles are important factors for methanol synthesis component, while the acid strength (weak to medium) and acid sites (both Lewis and Brønsted) as well as the textural (meso porosity) properties play critical roles for methanol dehydration component. Generally, zeolites due to their hydrophobic nature show a higher catalytic activity and stability than γ-Al_2O_3 even at lower reaction temperature and thus Cu-ZnO-Al_2O_3/zeolites are the most commonly used hybrid catalysts for the STD process. DME selectivity, yield, stability and extent of by-product formation were found to strongly depend on the topology of the zeolites. Moreover, the catalytic activities and reaction rates were correlated with the amount of acidic sites as well as surface area of metallic copper.

Adjustment of Cu metallic functions by adding transition metal promoters beneficially improves the dispersion and surface area of Cu nanoparticles. Also an efficient promoter on the hybridized bifunctional catalysts would reduce the rate of water gas shift reaction. Modification of methanol dehydration component with anions, alkali metals, transition metals, rare earth metals and composite oxides are excellent strategies to restructuring of the solid acid strength with the consequent improvement in DME selectivity. The experimental results showed that the overall DME synthesis rates can be determined by the relative ratio of methanol synthesis and methanol dehydration component along with the reaction parameters. The literature survey shows that the synergy between the active sites for methanol synthesis and the active sites for methanol dehydration plays an important role for catalyst activity and stability. However, the hybridized bifunctional catalysts can be partially deactivated as the individual components reacted to each other which leading to the detrimental interactions during the catalyst preparation or calcination stages. In addition, the simultaneous copper sintering (or aggregation), copper oxidation and ion exchange of the acidic sites with Cu ions causes the deactivation of the hybrid catalysts. Efficiently confining of copper nanoparticles within the ordered mesoporous alumina and zeolite matrixes were proposed as an efficient strategy to improve the catalyst stability in direct DME synthesis. Moreover, the zeolite capsule catalysts are capable of increasing the desired products selectivity by giving severe space confinement to the methanol intermediate and final DME product in tandem catalytic process. The studies on CO_2 hydrogenation to DME over the hybridized bifunctional catalysts were also reported with a lower DME yield as compared to the hydrogenation of CO to DME. Hydrogenation of the chemically inert CO_2 exhibits strong thermodynamic limitations and thus lower production rate of DME is inevitable. In addition, more water is produced by CO_2 hydrogenation via reverse water gas shift reaction which decreases the methanol synthesis reaction rate and catalyst deactivation as well. However, the two stage plasma-hybrid catalyst system displayed an improved yield of DME by maintaining the synergistic effect between the plasma and the hybrid catalyst.

The fundamental works done so far have important future industrial aspects and they can be extended in different directions. The scale up studies are needed over the benchmark Cu-ZnO-Al_2O_3/γ-Al_2O_3,zeolites catalysts for industrial applications. Although some significant advances have been made in the catalysts for hydrogenation of CO to DME, the new catalytic systems for CO_2 hydrogenation to DME require a further development due to a difficulty of understanding of strong limitation of thermodynamic equilibrium and fast catalyst deactivation. By looking at the future perspective for STD synthesis over those hybridized bifunctional catalysts or hybrid materials, more researches can be done for the development of novel catalysts by studying the different combinations of methanol synthesis catalysts and solid acid catalysts. Optimizing the catalyst structures and building kinetic models with density functional theory (DFT) studies on STD process

are also necessary for a precise understanding of reaction mechanisms. More focuses on utilizing CO_2 for DME synthesis offer an influential alternative to tackle both global climate changes and fossil fuel depletions since all carbon-containing fuels upon their combustion by forming chemically inert CO_2 can be revamped back into the fuel chains, thus it can close the energy loop cycles without emission of the global warming CO_2 gas.

Acknowledgements

The authors would like to acknowledge the financial support from the National Research Foundation (NRF) grant funded by the Korea government (NRF-2016M3D3A1A01913253). The work was also supported by the National Research Council of Science and Technology (NST) through Degree and Research Center (DRC) Program (2016).

References

[1] S. Lee, J.G. Speight, S.K. Loyalka, Handbook of Alternative Fuel Technologies, Taylor & Francis Group, 2007.
[2] A.J. McMichael, Bulletin of the World Health Organization, 2000.
[3] S.P. Teong, G. Yi, Y. Zhang, Green Chem. 16 (2014) 2015–2026.
[4] G.A. Olah, A. Goeppert, G.K.S. Prakash, Beyond Oil and Gas: The Methanol Economy, Wiley-VCH, 2009.
[5] A. Goeppert, M. Czaun, J.P. Jones, G.K.S. Prakash, G.A. Olah, Chem. Soc. Rev. 43 (2014) 7995–8048.
[6] J. Kopyscinski, T.J. Schildhauer, S.M.A. Biollaz, Fuel 89 (2010) 1763–1783.
[7] K. Takeishi, Biofuels 1 (2010) 217–226.
[8] (a) L. Pengmei, Y. Zhenhong, W. Chuangzhi, M. Longlong, C. Yong, T. Noritatsu, Energy Convers. Manage. 48 (2007) 1132–1139;
(b) J. Chang, Y. Fu, Z. Luo, Biomass Bioenergy 39 (2012) 67–72.
[9] R.M. Lopez, PhD Thesis, Imperial College London, 2014.
[10] K. Faungnawakij, K. Suriye, In New and Future Developments in Catalysis, Elsevier, 2013, pp. 79–104.
[11] (a) P.S.S. Prasad, J.W. Bae, S.–H. Kang, Y.–J. Lee, K.–W. Jun, Fuel Process. Technol. 89 (2008) 1281–1286;
(b) Y. Wang, C.J. Liu, Y.P. Zhang, Sci. Plasma, Tech 7 (2005) 2839–2841.
[12] California Environmental Protection Agency, California Dimethyl Ether Multimedia Evaluation, Tier 1, Feb, 2015.
[13] K. Omata, Y. Watanabe, T. Umegaki, G. Ishiguro, M. Yamada, Fuel 81 (2002) 1605–1609.
[14] T.H. Fleisch, A. Basu, M.J. Gradassi, J.G. Masin, Stud. Surf. Sci. Catal. 107 (1997) 117–125.
[15] H.J. Majunke, H. Mueller. German Pat. DE 3,307,091, 1984.
[16] I.E. Levine. US Pat. 4,892,561, 1990.
[17] ISI Web of knowledge [v.5.16.1] database; search keyword: direct synthesis of dimethyl ether and catalyst; search date: 06/12/2016.
[18] T.A. Semelsberger, R.L. Borup, H.L. Greene, J. Power Sources 156 (2006) 497–511.
[19] (a) C. Arcoumanis, C. Bae, R. Crookes, E. Kinoshita, Fuel 87 (2008) 1014–1030;
(b) S.H. Park, C.S. Lee, Energy Convers. Manage. 86 (2014) 848–863.
[20] E.S. Yoon, C. Han, Comput.-Aided Chem. Eng. 27 (2009) 169–175.
[21] G. Xiangbo, China Petrol. Proc. Petrochem. Technol. 12 (2010) 1–7.
[22] T.H. Fleisch, A. Basu, R.A. Sills, J. Nat. Gas Sci. Eng. 9 (2012) 94–107.
[23] S. Bhattacharya, K.B. Kabir, K. Hein, Prog. Energy Combust. Sci. 39 (2013) 577–605.
[24] J. Sun, G. Yang, Y. Yoneyama, N. Tsubaki, ACS Catal. 4 (2014) 3346–3356.
[25] Z. Azizi, M. Rezaeimanesh, T. Tohidian, M.R. Rahimpour, Chem. Eng. Process. 82 (2014) 150–172.
[26] J.W. Jeong, C.-Il Ahn, D.H. Lee, S.H. Um, J.W. Bae, Catal. Lett. 143 (2013) 666–672.
[27] S. Asthana, C. Samanta, A. Bhaumik, B. Banerjee, R.K. Voolapalli, B. Saha, J. Catal. 334 (2016) 89–101.
[28] (a) I. Wender, Fuel Process. Technol. 48 (1996) 189–297;
(b) M.H. Huang, H.M. Lee, K.C. Liang, C.C. Tzeng, W.H. Chen, Int. J. Hydrogen Energy 40 (2015) 13583–13593;
(c) E.F. Sousa-Aguiar, L.G. Appel, C. Mota, Catal. Today 101 (2005) 3–7.
[29] J.W. Bae, H.S. Potdar, S.-H. Kang, K.-W. Jun, Energy Fuels 22 (2008) 223–230.
[30] (a) A.T. Aguayo, J. Ereña, D. Mier, J.M. Arandes, M. Olazar, J. Bilbao, Ind. Eng. Chem. Res. 46 (2007) 5522–5530;
(b) Q. Ge, Y. Huang, F. Qiu, S. Li, Appl. Catal. A 167 (1998) 23–30;
(c) Z. Wang, J. Wang, J. Diao, Y. Jin, Chem. Eng. Technol. 24 (2001) 507–511.
[31] G.X. Qi, J.H. Fei, X.M. Zheng, Z.Y. Hou, Catal. Lett. 72 (2001) 121–124.
[32] W.H. Chen, B.J. Lin, H.M. Lee, M.H. Huang, Appl. Energy 98 (2012) 92–101.
[33] S. Lee, Methanol Synthesis Technology, CRC Press, Boca Raton, FL, 1990.
[34] M. Behrens, F. Studt, I. Kasatkin, S. Kühl, M. Hävecker, F. Abild-Pedersen, S. Zander, F. Girgsdies, P. Kurr, B.L. Kniep, M. Tovar, R.W. Fischer, J.K. Nørskov, R. Schlögl, Science 336 (2012) 893–897.
[35] M. Marchionna, M.D. Girolamo, L. Tagliabue, M.J. Spangler, T.H. Fleisch, Stud. Surf. Sci. Catal. 119 (1998) 539–544.
[36] H. Pines, W.O. Haag, J. Am. Chem. Soc. 82 (1960) 2471–2483.
[37] D. Sung, Y. Kim, E. Park, J. Yie, Res. Chem. Intermed. 36 (2010) 653–660.
[38] M. Trueba, S.P. Trasatti, Eur. J. Inorg. Chem. 17 (2005) 3393–3403.
[39] (a) A.C. Sofianos, M.S. Scurrell, Ind. Eng. Chem. Res. 30 (1991) 2372–2378;
(b) M. Xu, J.H. Lunsford, D.W. Goodman, A. Bhattacharyya, Appl. Catal. A 149 (1997) 289–301.
[40] T. Ennaert, J.V. Aelst, J. Dijkmans, R.D. Clercq, W. Schutyser, M. Dusselier, D. Verboekend, B.F. Sels, Chem. Soc. Rev. 45 (2016) 584–611.
[41] M. Guisnet, F. Ramôa, Les zéolithes: un nanomonde au service de la catalyse, EDP Sciences, Cedex, France, 2006.
[42] M. Niwa, N. Katada, K. Okumura, Characterization and Design of Zeolite Catalysts: Solid Acidity, Shape Selectivity and Loading Properties, 141, Springer Series in Materials Science, 2010.
[43] (a) A. Aho, N. Kumar, K. Eränen, T. Salmi, M. Hupa, D.Y. Murzin, Fuel 87 (2008) 2493–2501;
(b) Q. Xie, P. Chen, P. Peng, S. Liu, P. Peng, B. Zhang, Y. Cheng, Y. Wan, Y. Liu, R. Ruan, RSC Adv. 5 (2015) 26301–26307.
[44] Z. Li, J. Li, M. Dai, Y. Liu, D. Han, J. Wu, Fuel 121 (2014) 173–177.
[45] G.R. Moradi, S. Nosrati, F. Yaripor, Catal. Commun. 8 (2007) 598–606.
[46] M. Cai, A. Palčić, V. Subramanian, S. Moldovan, O. Ersen, V. Valtchev, V.V. Ordomsky, A.Y. Khodakov, J. Catal. 338 (2016) 227–238.
[47] (a) M. Gentzen, W. Habicht, D.E. Doronkin, J.-D. Grunwaldt, J. Sauer, S. Behrens, Catal. Sci. Technol. 6 (2016) 1054–1063;
(b) A. García-Trenco, E.R. White, M.S.P. Shaffer, C.K. Williams, Catal. Sci. Technol. 6 (2016) 4389–4397.
[48] R. Khoshbin, M. Haghighi, Catal. Sci. Technol. 4 (2014) 1779–1792.
[49] R. Ahmad, M. Hellinger, M. Buchholz, H. Sezen, L. Gharnati, C. Wöll, J. Sauer, M. Döring, J.-D. Grunwaldt, U. Arnold, Catal. Commun. 43 (2014) 52–56.
[50] G.R. Moradi, M. Nazari, F. Yaripour, Fuel Process. Technol. 89 (2008) 1287–1296.
[51] M. Stiefel, R. Ahmad, U. Arnold, M. Döring, Fuel Process. Technol. 92 (2011) 1466–1474.
[52] D. Wang, Y. Han, Y. Tan, N. Tsubaki, Fuel Process. Technol. 90 (2009) 446–451.
[53] G.-xin Jia, H.-bin Ma, Y.-sheng Tan, Y.-zhuo Han, Ind. Eng. Chem. Res. 44 (2005) 2011–2015.
[54] S. Papari, M. Kazemeini, M. Fattahi, J. Nat. Gas Chem. 21 (2012) 148–157.
[55] F. Hayer, H.B. -Davijany, R. Myrstad, A. Holmen, P. Pfeifer, H.J. Venvik, Chem. Eng. Process. 70 (2013) 77–85.
[56] S.B. Lee, W. Cho, D.K. Park, E.S. Yoon, Korean J. Chem. Eng. 23 (2006) 522–530.
[57] I. Sierra, J. Ereña, A.T. Aguayo, J.M. Arandes, M. Olazar, J. Bilbao, Appl. Catal. B 106 (2011) 167–173.
[58] J. Ereña, I. Sierra, M. Olazar, A.G. Gayubo, A.T. Aguayo, Ind. Eng. Chem. Res. 47 (2008) 2238–2247.
[59] H.J. Kim, H. Jung, K.Y. Lee, Korean J. Chem. Eng. 18 (2001) 838–841.
[60] H.W. Ham, M.H. Jeong, H.M. Koo, C.H. Chung, J.W. Bae, Reac. Kinet. Mech. Cat. 116 (2015) 173–189.
[61] J. Abu-Dahrieh, D. Rooney, A. Goguet, Y. Saih, Chem. Eng. J. 203 (2012) 201–211.
[62] H. Jung, S.M. Lee, D.R. Yang, K.D. Jung, Bull. Korean Chem. Soc. 36 (2015) 1221–1225.
[63] X.D. Peng, B.A. Toseland, R.P. Underwood, Stud. Surf. Sci. Catal. 111 (1997) 175–182.
[64] S.P. Naik, H. Du, H. Wan, V. Bui, J.D. Miller, W.W. Zmierczak, Ind. Eng. Chem. Res. 47 (2008) 9791–9794.
[65] E.J. Kim, N.-K. Park, G.B. Han, S.O. Ryu, T.J. Lee, Process Saf. Environ. Prot. 84 (2006) 469–475.
[66] A. García-Trenco, A. Martínez, Appl. Catal. A 493 (2015) 40–49.
[67] G.R. Moradi, R. Ghanei, F. Yaripour, React. Kinet. Catal. Lett. 92 (2007) 137–145.
[68] J.L. Li, X.G. Zhang, T. Inui, Appl. Catal. A 147 (1996) 23–33.
[69] S. Lee, A. Sardesai, Top. Catal. 32 (2005) 197–207.
[70] J.L. Li, X.G. Zhang, T. Inui, Appl. Catal. A 164 (1997) 303–311.
[71] R. Ahmad, D. Schrempp, S. Behrens, J. Sauer, M. Döring, U. Arnold, Fuel Process. Technol. 121 (2014) 38–46.
[72] A. Martinez, G. Prieto, A. Garcia-Tranco, E. Peris, Zeolites and Catalysis, in: J. Cejka, A. Corma, S. Zones (Eds.), Wiley-VCH, New York, 2010, p. 649.
[73] D. Jin, B. Zhu, Z. Hou, J. Fei, H. Lou, X. Zheng, Fuel 86 (2007) 2707–2713.
[74] S. Akarmazyan, PhD Thesis, University of Patras, 2015.
[75] T. Takeguchi, K.I. Yanagisawa, T. Inui, M. Inoue, Appl. Catal. A 192 (2000) 201–209.
[76] S.H. Lima, A.M.S. Forrester, L.A. Palacio, A.C. Faro Jr., Appl. Catal. A 488 (2014) 19–27.
[77] J. Xia, D. Mao, B. Zhang, Q. Chen, Y. Zhang, Y. Tang, Catal. Commun. 7 (2006) 362–366.
[78] D. Mao, W. Yang, J. Xia, B. Zhang, G. Lu, J. Mol. Catal. A 250 (2006) 138–144.
[79] R. Montesano, D. Chadwick, Catal. Commun. 29 (2012) 137–140.
[80] O.S. Joo, K.D. Jung, S.H. Han, Bull. Korean Chem. Soc. 23 (2002) 1103–1105.
[81] M.V. Twigg, M.S. Spencer, Top. Catal. 22 (2003) 191–203.
[82] M.V. Twigg, M.S. Spencer, Appl. Catal. A 212 (2001) 161–174.
[83] M. Kurtz, N. Bauer, C. Buscher, H. Wilmer, O. Hinrichsen, R. Becker, S. Rabe, K. Merz, M. Driess, R.A. Fischer, M. Muhler, Catal. Lett. 92 (2004) 49–52.

[84] S.H. Kang, J.W. Bae, H.S. Kim, G.M. Dhar, K.W. Jun, Energy Fuels 24 (2010) 804–810.
[85] A. Venugopal, J. Palgunadi, J.K. Deog, O.S. Joo, C.H. Shin, J. Mol. Catal. A 302 (2009) 20–27.
[86] F. Song, Y. Tan, H. Xie, Q. Zhang, Y. Han, Fuel Process. Technol. 126 (2014) 88–94.
[87] Y. Tan, H. Xie, H. Cui, Y. Han, B. Zhong, Catal. Today 104 (2005) 25–29.
[88] J. Palgunadi, I. Yati, K.D. Jung, Reac. Kinet. Mech. Cat. 101 (2010) 117–128.
[89] Q. Zhang, Y.Z. Zuo, M.H. Han, J.F. Wang, Y. Jin, F. Wei, Catal. Today 150 (2010) 55–60.
[90] J. Toyir, P.R. de la Piscina, J.L.G. Fierro, N. Homs, Appl. Catal. B 34 (2001) 255–266.
[91] D. Mao, W. Yang, J. Xia, B. Zhang, Q. Song, Q. Chen, J. Catal. 230 (2005) 140–149.
[92] S.C. Baek, S.H. Kang, J.W. Bae, Y.J. Lee, D.H. Lee, K.Y. Lee, Energy Fuels 25 (2011) 2438–2443.
[93] S. Allahyari, M. Haghighi, A. Ebadi, S. Hosseinzadeh, Ultrason. Sonochem. 21 (2014) 663–673.
[94] J.W. Jung, Y.J. Lee, S.H. Um, P.J. Yoo, D.H. Lee, K.W. Jun, J.W. Bae, Appl. Catal. B 126 (2012) 1–8.
[95] D. Astruc, F. Lu, J.R. Arazanes, Angew. Chem. Int. Ed. 44 (2005) 7852–7872.
[96] N.J. Brown, A. García-Trenco, J. Weiner, E.R. White, M. Allinson, Y. Chen, P.P. Wells, E.K. Gibson, K. Hellgardt, M.S.P. Shaffer, C.K. Williams, ACS Catal. 5 (2015) 2895–2902.
[97] (a) Z. Gao, L. Hao, W. Huang, K. Xie, Catal. Lett. 102 (2005) 139–141;
(b) Z. Gao, W. Huang, L. Yin, L. Hao, K. Xie, Catal. Lett. 127 (2009) 354–359.
[98] H. Ham, J. Kim, S.J. Cho, J.H. Choi, D.J. Moon, J.W. Bae, ACS Catal. 6 (2016) 5629–5640.
[99] C. Ahn, H.M. Koo, J.M. Jo, H.S. Roh, J.B. Lee, Y.J. Lee, E.J. Jang, J.W. Bae, Appl. Catal. B 180 (2016) 139–149.
[100] C. Ahn, Y.J. Lee, S.H. Um, J.W. Bae, Chem. Commun. 52 (2016) 4820–4823.
[101] H. Jiang, H. Bongard, W. Schmidt, F. Schüth, Microporous Mesoporous Mat. 164 (2012) 3–8.
[102] Y. Wang, Y. Chen, F. Yu, D. Pan, B. Fan, J. Ma, R. Li, J. Energy Chem. 25 (2016) 775–781.
[103] A. Bayat, T. Dogu, Ind. Eng. Chem. Res. 55 (2016) 11431–11439.
[104] L.-B. Sun, W.H. Tian, X.Q. Liu, J. Phys. Chem. C 113 (2009) 19172–19178.
[105] J.H. Kim, M.J. Park, S.J. Kim, O.S. Joo, K.D. Jung, Appl. Catal. A 264 (2004) 37–41.
[106] Y. Tavan, S.H. Hosseini, M. Ghavipour, M.R.K. Nikou, A. Shariati, Chem. Eng. Process. 73 (2013) 144–150.
[107] J.J. Spivey, Chem. Eng. Comm. 110 (1991) 123–142.
[108] F.S. Ramos, A.M.D. de Farias, L.E.P. Borges, J.L. Monteiro, M.A. Fraga, E.F. Sousa-Aguiar, L.G. Appel, Catal. Today 101 (2005) 39–44.
[109] Q. Xu, P. Lan, K. Huang, Y. Yan, Petrol. Sci. Technol. 29 (2011) 1080–1092.
[110] J. Fei, Z. Hou, B. Zhu, H. Lou, X. Zheng, Appl. Catal. A 304 (2006) 49–54.
[111] L. Wang, Y. Qi, Y. Wei, D. Fang, S. Meng, Z. Liu, Catal. Lett. 106 (2006) 61–66.
[112] D. Mao, J. Xia, Q. Chen, G. Lu, Catal. Commun. 10 (2009) 620–624.
[113] V.V. Ordomsky, M. Cai, V. Sushkevich, S. Moldovan, O. Ersen, C. Lancelot, V. Valtchev, A.Y. Khodakov, Appl. Catal. A 486 (2014) 266–275.
[114] A. García-Trenco, A. Vidal-Moya, A. Martínez, Catal. Today 179 (2012) 43–51.
[115] A. García-Trenco, A. Martínez, Appl. Catal. A 411–412 (2012) 170–179.
[116] A. García-Trenco, S. Valencia, A. Martínez, Appl. Catal. A 468 (2013) 102–111.
[117] A. García-Trenco, A. Martínez, Catal. Today 227 (2014) 144–153.
[118] R. Montesano, A. Narvaez, D. Chadwick, Appl. Catal. A 482 (2014) 69–77.
[119] J. Sun, G. Yang, Q. Ma, I. Ooki, A. Taguchi, T. Abe, Q. Xie, Y. Yoneyama, N. Tsubaki, J. Mater. Chem. A 2 (2014) 8637–8643.
[120] J. Xia, D. Mao, W. Tao, Q. Chen, Y. Zhang, Y. Tang, Microporous Mesoporous Mat. 91 (2006) 33–39.
[121] J. Hu, Y. Wang, C. Cao, D.C. Elliott, D.J. Stevens, J.F. White, Ind. Eng. Chem. Res. 44 (2005) 1722–1727.
[122] W.Z. Lu, L.H. Teng, W.D. Xiao, Chem. Eng. Sci. 59 (2004) 5455–5464.
[123] M. Jia, W. Li, H. Xu, S. Hou, Q. Ge, Appl. Catal. A 233 (2002) 7–12.
[124] R. Khoshbin, M. Haghighi, J. Renew. Sustain. Energy 7 (2015) 023127 (1-023127.19).
[125] G.R. Moradi, J. Ahmadpour, F. Yaripour, Chem. Eng. J. 144 (2008) 88–95.
[126] H. Zhang, W. Li, W. Xiao, Int. J. Chem. React. Eng. 10 (2012) 1–18.
[127] R. Khoshbin, M. Haghighi, P. Margan, Energy Convers. Manage. 120 (2016) 1–12.
[128] R. Khoshbin, M. Haghighi, Chem. Eng. Res. Des. 91 (2013) 1111–1122.
[129] J. Ereña, R. Garoña, J.M. Arandes, A.T. Aguayo, J. Bilbao, Catal. Today 107–108 (2005) 467–473.
[130] D. Mao, X. Guo, Energy Technol. 2 (2014) 882–888.
[131] Q.L. Xu, P. Lan, S.P. Zhang, T.C. Li, Y.J. Yan, Petrol. Sci. Technol. 29 (2011) 439–448.
[132] D. Mao, J. Xia, B. Zhang, G. Lu, Energy Convers. Manage. 51 (2010) 1134–1139.
[133] S.H. Kang, J.W. Bae, K.W. Jun, H.S. Potdar, Catal. Commun. 9 (2008) 2035–2039.
[134] J. Xia, D. Mao, B. Zhang, Q. Chen, Y. Tang, Catal. Lett. 98 (2004) 235–240.
[135] J.H. Flores, D.P.B. Peixoto, L.G. Appel, R.R. de Avillez, M.I. Pais da Silva, Catal. Today 172 (2011) 218–225.
[136] J.W. Bae, S.H. Kang, Y.J. Lee, K.W. Jun, Appl. Catal. B 90 (2009) 426–435.
[137] J.W. Bae, S.H. Kang, Y.J. Lee, K.W. Jun, J. Ind. Eng. Chem. 15 (2009) 566–572.
[138] Y.J. Lee, M.H. Jung, J.B. Lee, K.E. Jeong, H.S. Roh, Y.W. Suh, J.W. Bae, Catal. Today 228 (2014) 175–182.
[139] S. Allahyari, M. Haghighi, A. Ebadi, H.Q. Saeedi, J. Power Sources 272 (2014) 929–939.
[140] S. Allahyari, M. Haghighi, A. Ebadi, S. Hosseinzadeh, Energy Convers. Manage. 83 (2014) 212–222.
[141] S. Allahyari, M. Haghighi, A. Ebadi, H.Q. Saeedi, Int. J. Energy Res. 38 (2014) 2030–2043.
[142] S. Allahyari, M. Haghighi, A. Ebadi, Chem. Eng. J. 262 (2015) 1175–1186.
[143] G. Yang, N. Tsubaki, J. Shamoto, Y. Yoneyama, Y. Zhang, J. Am. Chem. Soc. 132 (2010) 8129–8136.
[144] G. Yang, M. Thongkam, T. Vitidsant, Y. Yoneyama, Y. Tan, N. Tsubaki, Catal. Today 171 (2011) 229–235.
[145] G. Yang, D. Wang, Y. Yoneyama, Y. Tan, N. Tsubaki, Chem. Commun. 48 (2012) 1263–1265.
[146] K. Pinkaew, G. Yang, T. Vitidsant, Y. Jin, C. Zeng, Y. Yoneyama, N. Tsubaki, Fuel 111 (2013) 727–732.
[147] R. Phienluphon, K. Pinkaew, G. Yang, J. Li, Q. Wei, Y. Yoneyama, T. Vitidsant, N. Tsubaki, Chem. Eng. J. 270 (2015) 605–611.
[148] R. Nie, H. Lei, S. Pan, L. Wang, J. Fei, Z. Hou, Fuel 96 (2012) 419–425.
[149] W. Yan, W. Wen-li, C. Yue-xian, Z. Jia-jun, L. Rui-feng, Fuel Chem. Technol. 41 (2013) 873–882.
[150] Y. Wang, W. Wang, Y. Chen, J. Ma, J. Zheng, R. Li, Chem. Lett. 42 (2013) 335–337.
[151] Y. Wang, W. Wang, Y. Chen, J. Ma, R. Li, Chem. Eng. J. 250 (2014) 248–256.
[152] J. Li, X. Pan, X. Bao, Chinese J. Catal. 36 (2015) 1131–1135.
[153] W. Ding, M. Klumpp, S. Lee, S. Reuß, S.A. Al-Thabaiti, P. Pfeifer, W. Schwieger, R. Dittmeyer, Chem. Ing. Tech. 87 (2015) 702–712.
[154] F.S.R. Barbosa, V.S.O. Ruiz, J.L.F. Monteiro, R.R. de Avillez, L.E.P. Borges, L.G. Appel, Catal. Lett. 126 (2008) 173–178.
[155] Y. Luan, H. Xu, C. Yu, W. Li, S. Hou, Catal. Lett. 125 (2008) 271–276.
[156] C. Zeng, J. Sun, G. Yang, I. Ooki, K. Hayashi, Y. Yoneyama, A. Taguchi, T. Abe, N. Tsubaki, Fuel 112 (2013) 140–144.
[157] M. Cai, V. Subramanian, V.V. Sushkevich, V.V. Ordomsky, A.Y. Khodakov, Appl. Catal. A 502 (2015) 370–379.
[158] Z. Li, J. Li, C. Yang, J. Wu, J. Nat. Gas Chem. 21 (2012) 360–365.
[159] J.H. Fei, M.X. Yang, Z.Y. Hou, X.M. Zheng, Energy Fuels 18 (2004) 1584–1587.
[160] J.H. Fei, X.J. Tang, Z.Y. Huo, H. Lou, X.M. Zheng, Catal. Commun. 7 (2006) 827–831.
[161] X.J. Tang, J.H. Fei, Z.Y. Hou, X.M. Zheng, H. Lou, Energy Fuels 22 (2008) 2877–2884.
[162] K. Sun, W. Lu, F. Qiu, S. Liu, X. Xu, Appl. Catal. A 252 (2003) 243–249.
[163] G.R. Moradi, M. Nazari, F. Yaripour, Chem. Eng. J. 140 (2008) 255–263.
[164] N. Khandan, M. Kazemeini, Aghaziarati, Catal. Lett. 129 (2009) 111–118.
[165] N. Khandan, M. Kazemeini, Aghaziarati, Petrochem Res. 1 (2012) 21–27.
[166] J. Xia, D. Mao, N. Xu, Q. Chen, Y. Zhang, Y. Tang, Chem. Lett. 33 (2004) 1456–1457.
[167] S.H. Ahn, S.H. Kim, K.B. Jung, H.S. Hahm, Korean J. Chem. Eng. 25 (2008) 466–470.
[168] S.H. Ahn, S.H. Kim, H.S. Hahm, Res. Chem. Intermed. 34 (2008) 793–801.
[169] R. Khoshbin, M. Haghighi, N. Asgari, Mater. Res. Bull. 48 (2013) 767–777.
[170] K.S. Yoo, J.H. Kim, M.J. Park, S.J. Kim, O.S. Joo, K.D. Jung, Appl. Catal. A 330 (2007) 57–62.
[171] A. Ateka, I. Sierra, J. Ereña, J. Bilbao, A.T. Aguayo, Fuel Process. Technol. 152 (2016) 34–45.
[172] G.A. Olah, A. Goeppert, G.K.S. Prakash, J. Org. Chem. 74 (2009) 487–498.
[173] (a) J. Ma, N. Sun, X. Zhang, N. Zhao, F. Xiao, W. Wei, Y. Sun, Catal. Today 148 (2009) 221–231;
(b) W.C. Chueh, C. Falter, M. Abbott, D. Scipio1, P. Furler, S.M. Haile1, A. Steinfeld, Science 330 (2010) 1797–1801.
[174] W. Wang, S. Wang, X. Ma, J. Gong, Chem. Soc. Rev. 40 (2011) 3703–3727.
[175] S. Sankaranarayanan, K. Srinivasan, Ind. J. Chem. A 51A (2012) 1252–1262.
[176] (a) K.W. Jun, K.S.R. Rao, M.H. Jung, K.W. Lee, Bull. Korean Chem. Soc. 19 (1998) 466–470;
(b) Z.Z. Qin, X.H. Zhou, T.M. Su, Y.X. Jiang, H.B. Ji, Catal. Commun. 75 (2016) 78–82.
[177] (a) F. Zha, H. Tian, J. Yan, Y. Chang, Appl. Surf. Sci. 285P (2013) 945–951;
(b) X. Zhou, T. Su, Y. Jiang, Z. Qin, H. Ji, Z. Guo, Chem. Eng. Sci. 153 (2016) 10–20.
[178] J.L. Tao, K.W. Jun, K.W. Lee, Appl. Organometal. Chem. 15 (2001) 105–108.
[179] (a) L. Li, D. Mao, J. Xiao, L. Li, X. Guo, J. Yu, Chem. Eng. Res. Des. 111 (2016) 100–108;
(b) F. Arena, L. Spadaro, O.D. Blasi, G. Bonura, F. Frusteri, Surf. Sci. Catal. 147 (2004) 385–390;
(c) G. Bonura, C. Cannilla, L. Frusteri, A. Mezzapica, F. Frusteri, Catal. Today 281 (2017) 337–344;
(d) K. Sun, W. Lu, M. Wang, X. Xu, Catal. Commun. 5 (2004) 367–370.
[180] Y.K. Park, S.W. Baek, S.K. Ihm, Prepr. Symp. Am. Chem. Soc., Div. Fuel Chem. 47 (2002) 293–294.
[181] S.P. Naik, T. Ryu, V. Bui, J.D. Miller, N.B. Drinnan, W. Zmierczak, Chem. Eng. J. 167 (2011) 362–368.
[182] (a) W.J. Shen, K.W. Jun, H.S. Choi, K.W. Lee, Korean J. Chem. Eng. 17 (2000) 210–216;
(b) W.H. Chen, C.L. Hsu, X.D. Wang, Energy 109 (2016) 326–340;
(c) G. Jia, Y. Tan, Y. Han, Ind. Eng. Chem. Res. 45 (2006) 1152–1159.
[183] (a) G. Bonura, M. Cordaro, L. Spadaro, C. Cannilla, F. Arena, F. Frusteri, Appl. Catal. B 140–141 (2013) 16–24;

(b) J. Ereia, I. Sierra, A.T. Aguayo, A. Ateka, M. Olazar, J. Bilbao, Chem. Eng. J. 174 (2011) 660–667.
[184] T. Su, X. Zhou, Z. Qin, H. Ji, ChemPhyChem 18 (2017) 299–309.
[185] R.J. da Silva, A.F. Pimentel, R.S. Monteiro, C.J.A. Mota, J. CO_2 Util. 15 (2016) 83–88.
[186] A.T. Aguayo, J. Ereña, I. Sierra, M. Olazar, J. Bilbao, Catal. Today 106 (2005) 265–270.
[187] R. Liu, H. Tian, A. Yang, F. Zha, J. Ding, Y. Chang, Appl. Surf. Sci. 345 (2015) 1–9.
[188] A. Bansode, A. Urakawa, J. Catal. 309 (2014) 66–70.
[189] Y. Zhang, D. Li, S. Zhang, K. Wang, J. Wu, RSC Adv. 4 (2014) 16391–16396.
[190] Y. Zhao, J. Chen, J. Zhang, J. Nat. Gas Chem. 16 (2007) 389–392.
[191] G. Wengui, W. Hua, W. Yuhao, G. Wei, J. Miaoyao, J. Rare Earths 31 (2013) 470–476.
[192] J.L. Dubois, K. Sayama, H. Arakawa, Chem. Lett. 21 (1992) 1115–1118.
[193] K.W. Jun, W.J. Shen, K.W. Lee, Bull. Korean Chem. Soc. 20 (1999) 993–998.
[194] F. Zha, J. Ding, Yue Chang, J. Ding, J. Wang, J. Ma, Ind. Eng. Chem. Res. 51 (2012) 345–352.
[195] G. Bonura, M. Cordaro, C. Cannilla, A. Mezzapica, L. Spadaro, F. Arena, F. Frusteri, Catal. Today 228 (2014) 51–57.
[196] Y. Zhang, D. Li, Y. Zhang, Y. Cao, S. Zhang, K. Wang, F. Ding, J. Wu, Catal. Commun. 55 (2014) 49–52.
[197] M.H. Zhang, Z.M. Liu, G.D. Lin, H.B. Zhang, Appl. Catal. A 451 (2013) 28–35.
[198] F. Frusteri, G. Bonura, C. Cannilla, G.D. Ferrante, A. Aloise, E. Catizzone, M. Migliori, G. Giordano, Appl. Catal. B 176–177 (2015) 522–531.
[199] T. Witoon, T. Permsirivanich, N. Kanjanasoontorn, C. Akkaraphataworn, A. Seubsai, K. Faungnawakij, C. Warakulwit, M. Chareonpanich, J. Limtrakul, Catal. Sci. Technol. 5 (2015) 2347–2357.
[200] S. Wang, D. Mao, X. Guo, G. Wu, G. Lu, Catal. Commun. 10 (2009) 1367–1370.
[201] R.W. Liu, Z.Z. Qin, H.B. Ji, T.M. Su, Ind. Eng. Chem. Res. 52 (2013) 16648–16655.
[202] Z.Z. Qin, X.H. Zhou, T.M. Su, Y.X. Jiang, H.B. Ji, Catal. Commun. 75 (2016) 78–82.
[203] O.O. Rivera, M.A. Baltanàs, N.C. -Martlnez, J. CO_2 Util. 9 (2015) 8–15.
[204] F.C.F. Marcos, J.M. Assaf, E.M. Assaf, Catal. Today 289 (2017) 173–180.
[205] (a) X. An, Y.Z. Zuo, Q. Zhang, D.Z. Wang, J.F. Wang, Ind. Eng. Chem. Res. 47 (2008) 6547–6554;
(b) N. Diban, A.M. Urtiaga, I. Ortiz, J. Ereña, J. Bilbao, A.T. Aguayo, Chem. Eng. J. 234 (2013) 140–148.
[206] F. Arena, K. Barbera, G. Italiano, G. Bonura, L. Spadaro, F. Frusteri, J. Catal. 249 (2007) 185–194.
[207] F. Arena, G. Italiano, K. Barbera, S. Bordiga, G. Bonura, L. Spadaro, F. Frusteri, Appl. Catal. A 350 (2008) 16–23.
[208] F. Frusteri, M. Cordaro, C. Cannilla, G. Bonura, Appl. Catal. B 162 (2015) 57–65.
[209] M. Aresta, A. Dibenedetto, E. Quaranta, J. Catal. 343 (2016) 2–45.
[210] Z.Z. Qin, T.M. Su, H.B. Ji, Y.X. Jiang, R.W. Liu, J.H. Chen, AIChE J. 61 (2015) 1613–1627.
[211] G. Bonura, F. Frusteri, C. Cannilla, G.D. Ferrante, A. Aloise, E. Catizzone, M. Migliori, G. Giordano, Catal. Today 277 (2016) 48–54.
[212] K. Saravanan, B. Tyagi, H.C. Bajaj, Catal. Sci. Technol. 2 (2012) 2512–2520.